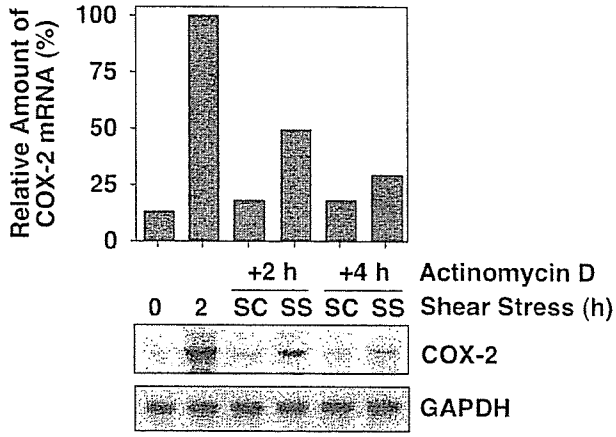


**Figure 4.** Effect of shear stress (SS) on COX-2 mRNA stability. HUVECs were exposed to SS of 15 dyne/cm$^2$ for 2 hours and then treated with actinomycin D (5 $\mu$g/mL) for a further 2 and 4 hours under static conditions (SC) or SS. Extracted RNAs (10 $\mu$g per lane) were analyzed by RNA blot analysis. Expression levels of COX-2 mRNAs were normalized with amounts of GAPDH mRNA and standardized to the value obtained at 2 hours of SS. Similar results were obtained by 2 additional experiments.

in the pattern of blood flow, such as turbulence, influence the PG species produced in endothelial cells should be examined.

In the present study, mutation analysis and gel-retardation assay indicated that the shear stress responsiveness of the COX-2 promoter was mainly dependent on CRE (−59/−53). The promoter activity of the fragment −1432/+59 was similar to that of the fragment −327/+59 induced by shear stress (data not shown), as reported in our previous studies using different stimuli.[11,16] Previous reports have indicated that CRE, CCAAT/enhancer binding protein-$\beta$ (same as NF-IL6), and activator protein-1 motifs play major roles in the shear stress induction of the COX-2 gene in osteoblasts, which is consistent with our results because of multiple binding activity of the CRE for CRE binding protein, CCAAT/enhancer binding proteins, and activator protein-1.[16,20] However, a triple mutation assay in Figure 3A suggested that other *cis*-acting elements also play a role in the COX-2 promoter activity.

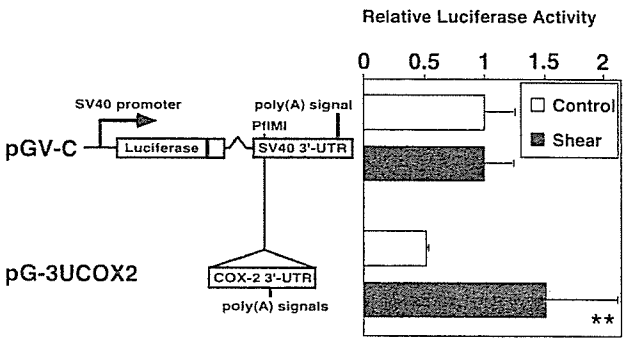


**Figure 5.** Involvement of the 3′-UTR of the COX-2 gene in response to shear stress. BAECs were transfected with Luc control vector pGV-C or pG-3UCOX2 containing 3′-UTR of the human COX-2 gene along with pCMV-$\beta$gal and pEGFP-N1. The transfected cells were subjected or not to shear stress at 15 dynes/cm$^2$ for 5 hours and then assayed for Luc and $\beta$-gal activities. The Luc activity was normalized to the $\beta$-gal activity and presented as the fold increase against the value obtained without shear stress of pGV-C. Data are mean±SD of 4 experiments. $^{**}P<0.01$ vs static control.

Actinomycin D chase experiments have indicated that shear stress stabilizes COX-2 mRNA levels in HUVECs. Similar experiments have also shown granulocyte-macrophage colony–stimulating factor (GM-CSF) mRNA also to be stabilized by shear stress,[45] although there was no induction of the promoter activity of the GM-CSF gene. The COX-2 and GM-CSF genes contain 17 and 8 copies, respectively, of the AUUUA motif in their 3′-UTRs.[33,34] Conserved AUUUA sequences have been identified within the 3′-UTR of many short-lived mRNAs and regulate their stability. The 3′-UTR of the COX-2 gene contains multiple copies of the AUUUA motif implicated in posttranscriptional regulation. Several investigators have shown that insertion of the 3′-UTR of the COX-2 gene into the 3′-UTR of the reporter gene alters its expression.[25–30]

The present study demonstrated for the first time that shear stress stabilizes COX-2 mRNA through the 3′-UTR of the COX-2 gene. Recently, it has been reported that the 3′-UTR of the murine COX-2 gene contains multiple regulatory elements that alter mRNA stability and translational efficiency even in the steady state.[30] On the other hand, the AUUUA motif found in GM-CSF mRNA has been considered not to function as a shear stress–responsive element, because protein binding to this motif was not influenced by shear stress.[45] Further study is necessary to resolve these issues.

## Acknowledgments

This study was partly supported by grants from the Ministry of Education, Science, Sports, and Culture, Japan (grants-in-aid for scientific research Nos. 11838021 and 13670110); from the Ministry of Health and Welfare, Japan (research grants for cardiovascular diseases Nos. 11C-1 and 12C-3); and from the Mochida Memorial Foundation for Medical and Pharmaceutical Research.

## References

1. Gimbrone MA Jr, Topper JN, Nagel T, Anderson KR, Garcia-Cardena G. Endothelial dysfunction, hemodynamic forces, and atherogenesis. *Ann N Y Acad Sci*. 2000;902:230–240.
2. Smith WL, Langenbach R. Why there are two cyclooxygenase isozymes. *J Clin Invest*. 2001;107:1491–1495.
3. Herschman HR. Function and regulation of prostaglandin synthase 2. *Adv Exp Med Biol*. 1999;469:3–8.
4. Vane JR, Bakhel YS, Botting RM. Cyclooxygenases 1 and 2. *Annu Rev Pharmacol Toxicol*. 1998;38:97–120.
5. Dubois RN, Abramson SB, Crofford L, Gupta RA, Simon LS, Van De Putte LB, Lipsky PE. Cyclooxygenase in biology and disease. *FASEB J*. 1998;12:1063–1073.
6. Oshima M, Dinchuk JE, Kargman SL, Oshima H, Hancock B, Kwong E, Trzaskos JM, Evans JF, Taketo MM. Suppression of intestinal polyposis in Apc delta716 knockout mice by inhibition of cyclooxygenase 2. *Cell*. 1996;87:803–809.
7. Morham SG, Langenbach R, Loftin CD, Tiano HF, Vouloumanos N, Jennette JC, Mahler JF, Kluckman KD, LedfordA, Lee CA, Smithies O. Prostaglandin synthase 2 gene disruption causes severe renal pathology in the mouse. *Cell*. 1995;83:473–482.
8. Dinchuk JE, Car BD, Focht RJ, Johnston JJ, Jaffee BD, Covington MB, Contel NR, Eng VM, Collins RJ, Czerniak PM, Gorry AG, Trzaskos JM. Renal abnormalities and an altered inflammatory response in mice lacking cyclooxygenase II. *Nature*. 1995;378:406–409.
9. Lim H, Paria BC, Das SK, Dinchuk JE, Langenbach R, Trzaskos JM, Dey SK. Multiple female reproductive failures in cyclooxygenase 2-deficient mice. *Cell*. 1997;91:197–208.

10. Topper JN, Cai J, Falb D, Gimbrone MA Jr. Identification of vascular endothelial genes differentially responsive to fluid mechanical stimuli: cyclooxygenase-2, manganese superoxide dismutase, and endothelial cell nitric oxide synthase are selectively up-regulated by steady laminar shear stress. *Proc Natl Acad Sci U S A*. 1996;93:10417–10422.
11. Inoue H, Umesono K, Nishimori T, Hirata Y, Tanabe T. Glucocorticoid-mediated suppression of the promoter activity of the cyclooxygenase-2 gene is modulated by expression of its receptor in vascular endothelial cells. *Biochem Biophys Res Commun*. 1999;254:292–298.
12. McAdam BF, Catella-Lawson F, Mardini IA, Kapoor S, Lawson JA, FitzGerald GA. Systemic biosynthesis of prostacyclin by cyclooxygenase (COX-2): the human pharmacology of a selective inhibitor of COX-2. *Proc Natl Acad Sci U S A*. 1999;96:272–277.
13. Taba Y, Sasaguri T, Miyagi M, Abumiya T, Miwa Y, Ikeda T, Mitsumata M. Fluid shear stress induces lipocalin-type prostaglandin $D_2$ synthase expression in vascular endothelial cells. *Circ Res*. 2000;86:967–973.
14. Sirois J, Simmons DL, Richards JS. Hormonal regulation of messenger ribonucleic acid encoding a novel isoform of prostaglandin endoperoxide H synthase in rat preovulatory follicles: induction in vivo and in vitro. *J Biol Chem*. 1992;267:11586–11592.
15. Inoue H, Nanayama T, Hara S, Yokoyama C, Tanabe T. The cyclic AMP response element plays an essential role in the expression of the human prostaglandin-endoperoxide synthase 2 gene in differentiated U937 monocytic cells. *FEBS Lett*. 1994;350:51–54.
16. Inoue H, Yokoyama C, Hara S, Tone Y, Tanabe T. Transcriptional regulation of human prostaglandin-endoperoxide synthase-2 gene by lipopolysaccharide and phorbol ester in vascular endothelial cells. *J Biol Chem*. 1995;270:24965–24971.
17. Yamamoto K, Arakawa T, Ueda N, Yamamoto S. Transcriptional roles of NF-κB and NF-IL-6 in the tumor necrosis factor α-dependent induction of cyclooxygenase-2 in MC3T3-E1 cells. *J Biol Chem*. 1995;270:31315–31320.
18. Inoue H, Tanabe T. Transcriptional role of the NF-κB site in the induction by lipopolysaccharide and suppression by dexamethasone of cyclooxygenase-2 in U937 cells. *Biochem Biophys Res Commun*. 1998;244:143–148.
19. Kim Y, Fischer SM. Transcriptional regulation of cyclooxygenase-2 in mouse skin carcinoma cells: regulatory role of CCAAT/enhancer-binding proteins in the differential expression of cyclooxygenase-2 in normal and neoplastic tissues. *J Biol Chem*. 1998;273:27686–27694.
20. Xie W, Herschman HR. v-src induces prostaglandin synthase 2 gene expression by activation of the c-Jun N-terminal kinase and the c-Jun transcription factor. *J Biol Chem*. 1995;270:27622–27628.
21. Murono S, Inoue H, Tanabe T, Joab I, Yoshizaki T, Furukawa M, Pagano JS. Induction of cyclooxygenase-2 by Epstein-Barr virus latent membrane protein 1 is involved in vascular endothelial growth factor production in nasopharyngeal carcinoma cells. *Proc Natl Acad Sci U S A*. 2001;98:6905–6910.
22. Saunders MA, Sansores-Garcia L, Gilroy DW, Wu KK. Selective suppression of CCAAT/enhancer-binding protein β binding and cyclooxygenase-2 promoter activity by salicylate in quiescent human fibroblast. *J Biol Chem*. 2001;276:18897–18904.
23. Inoue H, Tanabe T, Umesono K. Feedback control of cyclooxygenase-2 expression through PPARγ. *J Biol Chem*. 2000;275:28028–28032.
24. Ogasawara A, Arakawa T, Kaneda T, Takuma T, Sato T, Kaneko H, Kumegawa M, Hakeda Y. Fluid shear stress-induced cyclooxygenase-2 expression is mediated by C/EBPβ, cAMP-response element-binding protein, and AP-1 in osteoblastic MC3T3-E1 cells. *J Biol Chem*. 2001;276:7048–7054.
25. Srivastava SK, Tetsuka T, Daphna-Iken D, Morrison AR. IL-1β stabilized COX-2 mRNA in renal mesangial cells: role of 3′-untranslated region. *Am J Physiol*. 1994;267:F504–F508.
26. Newton R, Seybold J, Liu SF, Barnes PJ. Alternate COX-2 transcripts are differentially regulated: implications for post-transcriptional control. *Biochem Biophys Res Commun*. 1997;234:85–59.
27. Gou Q, Liu CH, Ben-Av P, Hla T. Dissociation of basal turnover and cytokine-induced transcript stabilization of the human cyclooxygenase-2 mRNA by mutagenesis of the 3′-untranslated region. *Biochem Biophys Res Commun*. 1998;242:508–512.
28. Dixon DA, Kaplan CD, McIntyre TM, Zimmerman GA, Prescott SM. Post-transcriptional control of cyclooxygenase-2 gene expression: the role of the 3′-untranslated region. *J Biol Chem*. 2000;275:11750–11757.
29. Xu K, Robida AM, Murphy TJ. Immediate-early MEK-1-dependent stabilization of rat smooth muscle cell cyclooxygenase-2 mRNA by Galpha(q)-coupled receptor signaling. *J Biol Chem*. 2000;275:23012–23019.
30. Cok SJ, Morrison AR. The 3′-untranslated region of murine cyclooxygenase-2 contains multiple regulatory elements that alter message stability and translational efficiency. *J Biol Chem*. 2001;276:23179–24185.
31. Kosaka C, Sasaguri T, Ishida A, Ogata J. Cell cycle arrest in the $G_2$ phase induced by phorbol ester and diacylglycerol in vascular endothelial cells. *Am J Physiol*. 1996;270:C170–C178.
32. Akimoto S, Mitsumata M, Sasaguri T, Yoshida Y. Laminar shear stress inhibits vascular endothelial cell proliferation by inducing cyclin-dependent kinase inhibitor p21(Sdi1/Cip1/Waf1). *Circ Res*. 2000;86:185–190.
33. Kosaka T, Miyata A, Ihara H, Hara S, Sugimoto T, Takeda O, Takahashi E, Tanabe T. Characterization of the human gene (PTGS2) encoding prostaglandin-endoperoxide synthase 2. *Eur J Biochem*. 1994;221:889–897.
34. Shaw G, Kamen R. A conserved AU sequences from 3′ untranslated region of GM-CSF mRNA mediates selective mRNA degradation. *Cell*. 1986;46:659–667.
35. Sach AB. Messenger RNA degradation in eukaryotes. *Cell*. 1993;74:413–421.
36. Okahara K, Sun B, Kambayashi J. Upregulation of prostacyclin synthesis-related gene expression by shear stress in vascular endothelial cells. *Arterioscler Thromb Vasc Biol*. 1998;18:1922–1926.
37. Feng Y, Yang JH, Huang H, Kennedy SP, Turi TG, Thompson JF, Libby P, Lee RT. Transcriptional profile of mechanically induced genes in human vascular smooth muscle cells. *Circ Res*. 1999;85:1118–1123.
38. Murakami M, Kambe T, Shimbara S, Kudo I. Functional coupling between various phospholipase $A_2$s and cyclooxygenases in immediate and delayed prostanoid biosynthetic pathways. *J Biol Chem*. 1999;274:3103–3115.
39. Ueno N, Murakami M, Tanioka T, Fujimori K, Tanabe T, Urade Y, Kudo I. Coupling between cyclooxygenase, terminal prostanoid synthase, and phospholipase $A_2$. *J Biol Chem*. 2001;276:34918–34927.
40. Belton O, Byrne D, Kearney D, Leahy A, Fitzgerald DJ. Cyclooxygenase-1 and -2–dependent prostacyclin formation in patients with atherosclerosis. *Circulation*. 2000;102:840–845.
41. Sebaldt RJ, Sheller JR, Oates JA, Roberts LJ II, FitzGerald GA. Inhibition of eicosanoid biosynthesis by glucocorticoids in humans. *Proc Natl Acad Sci U S A*. 1990;87:6974–6978.
42. Miwa Y, Sasaguri T, Inoue H, Taba Y, Ishida A, Abumiya T. 15-Deoxy-$\Delta^{12,14}$-prostaglandin $J_2$ induces $G_1$ arrest and differentiation marker expression in vascular smooth muscle cells. *Mol Pharmacol*. 2000;58:837–844.
43. Schonbeck U, Sukhova GK, Graber P, Coulter S, Libby P. Augmented expression of cyclooxygenase-2 in human atherosclerotic lesions. *Am J Pathol*. 1999;155:1281–1291.
44. Baker CS, Hall RJ, Evans TJ, Pomerance A, Maclouf J, Creminon C, Yacoub MH, Polak JM. Cyclooxygenase-2 is widely expressed in atherosclerotic lesions affecting native and transplanted human coronary arteries and colocalizes with inducible nitric oxide synthase and nitrotyrosine particularly in macrophages. *Arterioscler Thromb Vasc Biol*. 1999;19:646–655.
45. Kosaki K, Ando J, Korenaga R, Kurokawa T, Kamiya A. Fluid shear stress increases the production of granulocyte-macrophage colony-stimulating factor by endothelial cells via mRNA stabilization. *Circ Res*. 1998;82:794–802.

MOLECULAR AND CELLULAR BIOLOGY, Sept. 2002, p. 6582–6591 Vol. 22, No. 18
0270-7306/02/$04.00+0 DOI: 10.1128/MCB.22.18.6582–6591.2002


# Activation of Rac and Cdc42 Video Imaged by Fluorescent Resonance Energy Transfer-Based Single-Molecule Probes in the Membrane of Living Cells

Reina E. Itoh,[1] Kazuo Kurokawa,[1] Yusuke Ohba,[1,2] Hisayoshi Yoshizaki,[1,2] Naoki Mochizuki,[3] and Michiyuki Matsuda[1]*

*Department of Tumor Virology, Research Institute for Microbial Diseases, Osaka University, Osaka 565-0871,[1] and CREST, Japan Science and Technology Cooperation,[2] and Department of Structural Analysis, National Cardiovascular Research Institute,[3] Osaka 565-8565, Japan*

Received 17 January 2002/Returned for modification 18 March 2002/Accepted 20 June 2002

**Rho family G proteins, including Rac and Cdc42, regulate a variety of cellular functions such as morphology, motility, and gene expression. We developed fluorescent resonance energy transfer-based probes which monitored the local balance between the activities of guanine nucleotide exchange factors and GTPase-activating proteins for Rac1 and Cdc42 at the membrane. These probes, named Raichu-Rac and Raichu-Cdc42, consisted of a Cdc42- and Rac-binding domain of Pak, Rac1 or Cdc42, a pair of green fluorescent protein mutants, and a CAAX box of Ki-Ras. With these probes, we video imaged the Rac and Cdc42 activities. In motile HT1080 cells, activities of both Rac and Cdc42 gradually increased toward the leading edge and decreased rapidly when cells changed direction. Under a higher magnification, we observed that Rac activity was highest immediately behind the leading edge, whereas Cdc42 activity was most prominent at the tip of the leading edge. Raichu-Rac and Raichu-Cdc42 were also applied to a rapid and simple assay for the analysis of putative guanine nucleotide exchange factors (GEFs) and GTPase-activating proteins (GAPs) in living cells. Among six putative GEFs and GAPs, we identified KIAA0362/DBS as a GEF for Rac and Cdc42, KIAA1256 as a GEF for Cdc42, KIAA0053 as a GAP for Rac and Cdc42, and KIAA1204 as a GAP for Cdc42. In conclusion, use of these single-molecule probes to determine Rac and Cdc42 activity will accelerate the analysis of the spatiotemporal regulation of Rac and Cdc42 in a living cell.**

Ras superfamily G proteins function as molecular switches in a variety of signaling cascades (51). Among them, Rho family G proteins, including Rho, Rac, and Cdc42, are involved in the regulation of a variety of cellular processes, probably through actin cytoskeleton reorganization (1, 9, 13, 48). In a pioneering work by Nobes and Hall, it was shown that Rho regulates the assembly of the actin stress fiber, that Rac induces lamellipodia and membrane ruffles, and that Cdc42 triggers filopodium formation (41).

Rho family G proteins are regulated by three classes of protein, guanine nucleotide exchange factor (GEF), GTPase-activating protein (GAP), and guanine nucleotide dissociation inhibitor (GDI) (51). GEF promotes the exchange of GDP with GTP, which results in the binding of the G proteins to their effector proteins. A typical GEF protein of the Rho family of G proteins consists of a Dbl homology (DH) domain, which exhibits GEF activity, and additional domains that mediate interactions with peptides or lipids. DOCK180, originally isolated as a protein bound to adapter protein Crk (14), also promotes guanine nucleotide exchange of Rac, although it does not contain the DH domain (20). The GTP on the activated Rho family G protein is hydrolyzed in the presence of GAP to resume the GDP-bound inactive state. GDI not only competes with GEF but also holds the Rho family G proteins in the cytoplasm (43). Therefore, the dissociation of GDI is a prerequisite for the membrane association and activation of the Rho family G proteins. ERM family proteins, which are involved in cell-to-cell interaction, release Rho from RhoGDI, translocating Rho from the cytoplasm to membrane (50). Recently, del Pozo and colleagues have shown that integrin stimulation triggers the release of Rac from RhoGDI (5), showing for the first time the involvement of RhoGDI in Rac signaling.

Fluorescent resonance energy transfer (FRET) is a nonradiative transfer of energy between two fluorophores that are placed in close vicinity and in a proper relative angular orientation. Variants of green fluorescent protein (GFP) provide genetically encoded fluorophores that serve as the donor and the acceptor in FRET (15, 33, 35). With the GFP variants and FRET technology, several intracellular events have been visualized in a living cell. Activations of factor Xa and caspases have been monitored by the use of probes in which protease-sensitive peptides are placed between the pair of GFP variants (27, 33, 56). In these probes, activated proteases cleave the probes to dissociate the donor from the acceptor, terminating FRET. In other examples, two GFP variants are fused to a pair of proteins which form a dimer upon stimulation. The binding of Bcl-2 to Bax and the binding of transcription factor Pit-1 to Ets-1 have been demonstrated by detecting FRET between the two GFP variants (4, 28). To overcome the difficulty in controlling the relative expression levels of the two GFP variants in a cell, several research groups have developed single-molecule probes, in which the monitor peptides are sandwiched with the two GFP variants. In these probes, FRET efficiency

* Corresponding author. Mailing address: Department of Tumor Virology, Research Institute for Microbial Diseases, Osaka University, Yamadaoka, Suita-shi, Osaka 565-0871, Japan. Phone: 81-6-6879-8316. Fax: 81-6-6879-8314. E-mail: matsudam@biken.osaka-u.ac.jp.

between the two GFP variants varies depending on either the phosphorylation of (25, 37) or calcium binding to (34, 47) the monitor peptide.

Recently, activation of Rac has been successfully monitored by FRET technology. Kraynov and colleagues used Cdc42- and Rac-interactive binding motif (CRIB) of PAK labeled with Alexa 546 as the acceptor and GFP-tagged Rac as the donor of FRET (24). In a motile Swiss 3T3 cell microinjected with the pair of probes, Kraynov et al. observed an increasing gradient of Rac activity toward the leading edge. Graham and his colleagues expressed CRIB of PAK between two GFP variants (12). Upon binding to the active Rac in vitro, the probe decreases the efficiency of FRET between the two GFP variants.

We have previously reported a probe, called Ras and interacting chimeric unit (Raichu), for monitoring the Ras family G proteins (36). This probe consists of Ras, the Ras-binding domain of Raf, and yellow-emitting (YFP) and cyan-emitting (CFP) GFP mutants. Upon activation of Ras, the binding to Raf increases the efficiency of FRET between CFP and YFP. With Raichu, growth factor-induced activation of Ras and another Ras family G protein, Rap1, in living cells was video imaged. Here, we report on probes named Raichu-Rac and Raichu-Cdc42, which are derived from Raichu and which are applicable to the video imaging of active Rac and Cdc42, respectively. Using these probes, we show that the distributions of active Rac and Cdc42 mostly overlap each other but that high activity at the tip of the leading edge is specific to Cdc42.

## MATERIALS AND METHODS

**Plasmids.** pRaichu-Ras and pRacihu-Rap1 have been described previously (36). pRaichu-Rac and pRaichu-Cdc42 were constructed using essentially the same procedure as was used to construct pRaichu-Ras (36). From the amino terminus, Raichu-Rac consists of YFP (amino acids [aa] 1 to 239), a spacer (Leu-Asp), CRIB of PAK1 (aa 68 to 150), a spacer (Ser-Gly-Gly-Thr-Gly-Gly-Gly-Gly-Thr), Rac1 (aa 1 to 176), a spacer (Gly-Gly-Arg), CFP (aa 1 to 237), a spacer (Gly-Arg-Ser-Arg), and the CAAX box of $K_i$-Ras (aa 169 to 188) (Fig. 1A). In this study, we used modified YFP (Thr66Gly, Val69Leu, Ser73Ala, Aln70Lys, and Thr204Tyr) and CFP (Lys27Arg, Tyr67Trp, Asp130Gly, Asn147Iso, Met154Thr, Val164Ala, Asn165His, and Ser176Gly) as the acceptor and the donor, respectively. In Raichu-Cdc42, Rac1 was replaced with Cdc42 (aa 2 to 176). In proteins denoted by suffixes V12, N17, and Y40C, $Gly^{12}$, $Thr^{17}$, $Tyr^{40}$ of Rac1 or Cdc42 were replaced with Val, Asn, and Cys, respectively. pRaichu-CRIB was generated by removing the coding sequence of Rac1 from pRaichu-Rac. cDNAs of KIAA0053, KIAA0362, KIAA0793, KIAA1204, KIAA1256, and KIAA1391 were obtained from the Kazusa DNA Institute, Kisarazu, Japan. Synthesized cDNA of dsFP593 (8) was obtained from A. Miyawaki at the Brain Science Institute, RIKEN, Wako-shi, Japan. pIRM21 is an expression vector derived from pCAGGS (40) and contained the internal ribosomal entry site and the coding region of dsFP593 at the 3′ side of the multiple cloning site. Coding sequences of the KIAA proteins were subcloned into the cloning site of pIRM21. pCAGGS-mSos (11), pCAGGS-RasGRF1 (11), and pCAGGS-myc-DOCK180 (14) have been described previously. pSRα-Vav (18) and pcDNA3-HA-Tiam1(C1199) (30) were obtained from H. Mano at Jichi Medical School and J. Collard at The Netherlands Cancer Institute, respectively. In pCXN2-Flag-Rac and pCXN2-Flag-Cdc42, coding regions of human Rac1 and human Cdc42, respectively, were subcloned into eukaryotic expression vector pCXN2-Flag (40). Similarly, the coding regions of Rac1 and Cdc42 were subcloned into pCAGGS-EGFP (42) to generate pCAGGS-EGFP-Rac1 and pCAGGS-EGFP-Cdc42. In proteins denoted by suffixes Q61L and Q63L, $Gln^{61}$ of Rac1 and Cdc42 and $Gln^{63}$ of RhoA were replaced with Leu.

**Recombinant adenoviruses.** Recombinant adenoviruses encoding Raichu-Ras, Raichu-Rap1, Raichu-Rac, and Raichu-Cdc42 were generated by the use of the Adeno-X expression system (Clontech), according to the manufacturer's instructions. First, coding regions of the probes were subcloned into pShuttle by restriction enzyme cleavage and ligation. Then, the expression units including the coding regions of the probes were cleaved out from these pShuttle-derived vectors by *PI-SceI* and *I-CeuI* and ligated with pAdeno-X cleaved with the same restriction enzymes. From these pAdeno-X-derived vectors, the genomes of the recombinant adenoviruses were cleaved out by *PacI* (New England Biolabs) and transfected into HEK293 cells. After 10 to 14 days, cells were harvested to propagate recombinant adenoviruses.

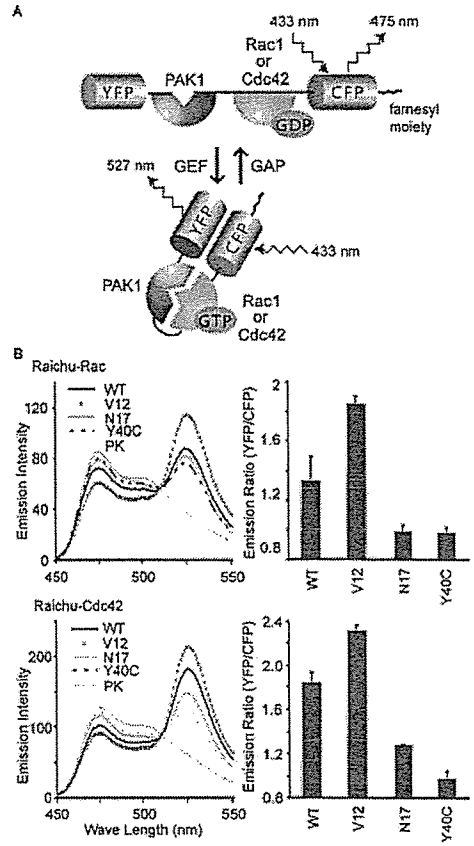


FIG. 1. Fluorescence profiles of Raichu-Rac and Raichu-Cdc42. (A) Schematic representations of Raichu-Rac and Raichu-Cdc42 bound to GDP or GTP. When Rac1 or Cdc42 is bound to GDP, fluorescence of 475 nm emanates from CFP with excitation at 433 nm. When Rac1 or Cdc42 is bound to GTP, intramolecular binding to PAK1 brings YFP into close proximity to CFP, which causes FRET and fluorescence of 527 nm from YFP. (B) 293T cells expressing Raichu-Rac and Raichu-Cdc42 were lysed and analyzed with a fluorescence spectrometer at an excitation wavelength of 433 nm. WT, V12, N17, and Y40C, wild type, constitutively active mutant, dominant-negative mutant, and effector mutant, respectively. The lysates of the wild type were further treated with proteinase K (PK), which cleaved the probes between YFP and CFP. We used emission intensities of CFP at 475 nm and of YFP at 530 nm to calculate the emission ratio, YFP/CFP (right). Experiments were performed in duplicate, and data are shown with standard deviations. Representative results from three independent experiments are shown.

**Cells and antibodies.** COS-1, HEK293, and HT1080 cells were purchased from the American Type Culture Collection or the Japan Cell Resource Bank. 293T cells were a gift from B. J. Mayer (University of Connecticut). Cells were maintained in Dulbecco's modified Eagle medium supplemented with 10% fetal bovine serum. Anti-GFP rabbit serum was developed in our laboratory (36). The anti-Flag M2 monoclonal antibody was purchased from Sigma.

**Protein expression, in vitro spectroscopy, and immunoblotting.** Plasmids were transfected into 293T cells by the calcium phosphate coprecipitation method. Thirty-six hours later, cells were harvested in lysis buffer (20 mM Tris-HCl [pH 7.5], 100 mM NaCl, 0.5% Triton X-100, 5 mM $MgCl_2$) and clarified by centrifugation. A fluorescence spectrum was obtained by use of an excitation wave-

length of 433 nm with an FP-750 spectrofluorometer (JASCO, Tokyo, Japan). For the demonstration of FRET, the cell lysates were incubated with 100 μg of proteinase K/ml at 37°C for 10 min and analyzed with a spectrometer.

**Analysis of guanine nucleotides bound to G proteins.** Guanine nucleotides bound to Raichu-Rac, Raichu-Cdc42, Flag-Rac, and Flag-Cdc42 were analyzed essentially as described previously (29). Briefly, 293T cells that had been transfected with plasmids for 36 h were labeled with $^{32}P_i$ in phosphate-free minimal essential medium (Life Technologies, Inc.) for 4 h. Cells were lysed in lysis buffer and clarified by centrifugation. Raichu-Rac and Raichu-Cdc42 were immunoprecipitated with an anti-GFP antibody, and Flag-tagged proteins were immunoprecipitated with an anti-Flag M2 monoclonal antibody. The immunoprecipitates were boiled and analyzed by thin-layer chromatography (TLC). The amount of $^{32}P_i$-labeled guanine nucleotides was quantitated with a BAS-1000 image analyzer (Fuji Film, Tokyo, Japan).

**Imaging of HT1080 cells.** HT1080 cells were transfected with plasmids with FuGene6 (Roche). Forty-eight hours after transfection, cells were imaged on an Olympus IX70 inverted microscope equipped with a cooled charge-coupled device camera, CoolSNAP HQ (Roper Scientific, Trenton, N.J.), controlled by MetaMorph software (Universal Imaging, West Chester, Pa.) (34, 36). For dual-emission ratio imaging of Raichu-Rac and Raichu-Cdc42, we used a 440AF21 excitation filter, a 455DRLP dichroic mirror, and two emission filters, 480AF30 for CFP and 535AF25 for YFP (Omega Optical Inc., Brattleboro, Vt.). Cells were illuminated with a 75-W xenon lamp through a 10% neutral density (ND) filter (Omega Optical Inc.) and a 60× oil immersion objective lens. The exposure time was 0.5 s when binning was set to 3 by 3. After background subtraction, the ratio image of YFP/CFP was created with the MetaMorph software and used to represent FRET efficiency. For the photobleaching experiment, cells were illuminated without an ND filter for 10 min. In this experiment, we used an MX510 excitation filter (Asahi Spectra Co., Tokyo, Japan).

**Imaging of moving HT1080 cells.** HT1080 cells were infected with recombinant adenoviruses as described previously (17) or transfected with plasmids by using FuGene6 (Roche). Forty-eight hours after infection or transfection, cells were replated onto a 35-mm-diameter collagen-coated glass base dish (Asahi Techno Glass Co., Tokyo, Japan). Beginning 1 h after replating, cells were imaged every 2 min for 2 h as already described.

**Analysis of GEF and GAP activity in 96-well plates.** COS-1 cells were plated to collagen-coated, glass bottom 96-well plates (Asahi Techno Glass Co.). Cells in each well were transfected with 50 ng of pRaichu-Rac or pRaichu-Cdc42 in combination with 100 ng of expression vectors encoding GEFs or GAPs with Polyfect (Qiagen). Eight wells were used for each sample. After 24 h, cells were fed with serum-free minimal essential medium and incubated for an additional 6 h, followed by imaging as already described, except that a 10× objective lens was used. From a single viewing field, FRET images of more than 30 cells were routinely obtained by using the autothreshold function of Metamorph. Values of area and fluorescence intensity for each cell were saved after background reduction. Further analysis was performed with Excel software (Microsoft). The following five steps were automated by a custom-made macro program that ran on the Excel program. First, data from cellular debris or aggregated cells were automatically removed by gating with area values. Second, the ratio of fluorescent intensity of YFP to that of CFP was calculated for each cell. Third, the average of the YFP/CFP ratio was calculated for each well. Fourth, the average and standard deviation were calculated from the YFP/CFP ratios for the eight wells that were transfected with the same set of plasmids. Finally, these data were used to draw a bar graph.

**Nucleotide sequence accession numbers.** The nucleotide sequences of the coding regions of pRaichu-Rac and pRaichu-Cdc42 were deposited in the DDBJ/EMBL/GenBank data base with accession no. AB074145 and AB074146, respectively.

## RESULTS

**In vivo probes for Rac and Cdc42 activities.** We designed a protein named Raichu-Rac that consisted of Rac1, CRIB of PAK, and the pair of YFP and CFP (Fig. 1A). At the carboxy terminus, the CAAX box of $K_i$-Ras was fused to locate the probe to the membrane. In this probe, we expected that the intramolecular binding of GTP-Rac1 to CRIB brought CFP close to YFP, increasing FRET from CFP to YFP. By replacing Rac1 with Cdc42, we also made a probe named Raichu-Cdc42. To examine whether GTP loading increased FRET efficiency, we prepared several mutants. In the mutants denoted with the suffix V12, $Gly^{12}$ was replaced with Val to inactivate the GTPase activity, resulting in the increased GTP loading in the mutants. In N17 mutants, $Thr^{17}$ was replaced with Asn; this mutation is known to reduce the affinity of G proteins for guanine nucleotides (32). In Y40C mutants, Cys was substituted for $Tyr^{40}$ in the effector domain of Rac or Cdc42, which is essential for the binding to Pak1 (26).

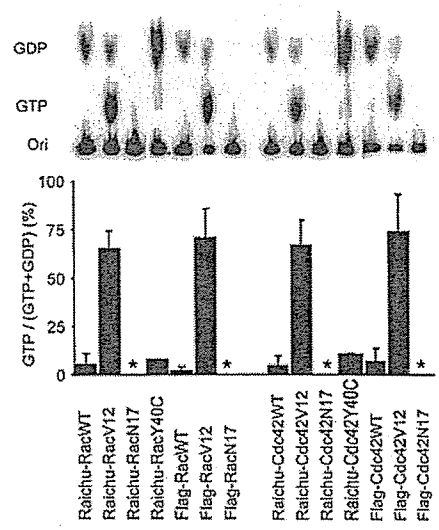


FIG. 2. GTP/GDP loading of Raichu-Rac and Raichu-Cdc42. 293T cells expressing Raichu-Rac, Raichu-Cdc42, Flag-tagged Rac, and Flag-tagged Cdc42 were labeled with $^{32}P_i$. The G proteins were precipitated with either anti-GFP rabbit serum or an anti-Flag monoclonal antibody, followed by TLC analysis. GTP and GDP were quantitated with a BAS-1000 image analyzer, and values of GTP/(GTP + GDP) with standard deviations were plotted. Asterisks indicate that no $^{32}P_i$-labeled guanine nucleotides were detected.

The probes were expressed in 293T cells, and their fluorescence emission profiles were obtained by the use of an excitation wavelength of 433 nm (Fig. 1B). Because FRET was most typically observed as an increase in an emission peak of 530 nm and a decrease in an emission peak of 475 nm, the emission ratio of 530 nm/475 nm is used to represent the FRET efficiency. As shown in Fig. 1B, right, the emission ratios for wild-type Raichu-Rac and Raichu-Cdc42 were lower than those for V12 mutants and higher than those for the N17 and Y40C mutants. The results demonstrated that increases in the emission ratios of Raichu-Rac and Raichu-Cdc42 reflected the binding of GTP-Rac and GTP-Cdc42 to CRIB. The cell lysates were further incubated with proteinase K, which cleaved the probes between YFP and CFP. The disappearance of the 530-nm peak confirmed FRET from CFP to YPF in the absence of proteinase K (Fig. 1B, left).

**GTP loading of the probes and the authentic G proteins.** To examine whether the GTP loading on Raichu probes correlated with those of the authentic proteins, 293T cells expressing Raichu-Rac, Flag-Rac, Raichu-Cdc42, or Flag-Cdc42 were labeled with $^{32}P_i$. Then, the labeled recombinant G proteins were immunoprecipitated, and the guanine nucleotides bound to them were analyzed by TLC (Fig. 2). The amount of GTP on Raichu-Rac-WT, Flag-Rac-WT, and Raichu-Rac-Y40C was

less than 10%, whereas the amount of GTP on Raichu-Rac-V12 and Flag-Rac-V12 was about 80% (Fig. 2, left). In Rac N17 mutants, the binding of guanine nucleotides was not detectable, which reflected the reduced affinity for the guanine nucleotides due to the $Asn^{17}$ mutation (7). Very similar results were obtained with Raichu-Cdc42 and Flag-Cdc42 (Fig. 2, right). These results validated the use of Raichu-Rac and Raichu-Cdc42 for monitoring Rac and Cdc42 activities in living cells.

**Imaging of Rac1 and Cdc42 activities in HT1080 cells.** Next, we used Raichu-Rac and Raichu-Cdc42 for cell imaging. HT1080 cells expressing Raichu-Rac or Raichu-Cdc42 were imaged for YFP (535 ± 12 nm) and CFP (480 ± 15 nm) with an excitation wavelength of 440 ± 10 nm (Fig. 3A). In both the YFP and CFP images, Raichu-Rac and Raichu-Cdc42 were detected diffusely within the cells, suggesting that they were localized mostly to the plasma membrane via the farnesyl moiety at the carboxyl terminus (Fig. 3A). The YFP/CFP ratio image was used to show the FRET efficiency in the intensity-modulated display mode.

In contrast to Raichu-Rac and Raichu-Cdc42, the authentic Rac1 and Cdc42 tagged with enhanced GFP (EGFP) were condensed around the nucleus (Fig. 3A). This distribution agreed with the cytoplasmic localization of GDP-Rac1 and GDP-Cdc42 coupled with RhoGDI (43). Thus, for the interpretation of the following image data, we emphasize that Raichu-Rac and Raichu-Cdc42 do not directly detect active Rac1 and Cdc42 but that they image the local balance of GEFs and GAPs for Rac1 and Cdc42 at the membrane compartments.

The occurrence of FRET in the living cells was confirmed by a photobleaching experiment as described previously (36). Intensities of both YFP and CFP were monitored before and after photobleaching. As expected, photobleaching of YFP resulted in a marked increase in CFP intensity (Fig. 3B).

**Activities of Rac, Cdc42, Ras, and Rap1 in motile HT1080 cells.** To understand the role of Rac and Cdc42 in cell migration, we examined the activities of Rac, Cdc42, Ras, and Rap1 in motile HT1080 cells that were infected with the recombinant adenoviruses encoding the Raichu probes. All of the cell images presented below are extracted from video images that are presented on our website (http://www-tv/biken.osaka-u.ac.jp/rei/).

For the video imaging of HT1080 cells for up to several hours, we minimized the exposure time to prevent YFP from photobleaching. Consequently, we had to compromise with the resolution of the images and fluctuation of the ratio data of each pixel. Therefore, the mosaic of ratio images was made up of pixels from blue to red, which corresponded from the lowest to the highest FRET efficiency. We interpreted the increasing number of red pixels toward the leading edge as reflecting the gradual increase in Rac activity (Fig. 4). When the cell changed direction and the plasma membrane started to withdraw, the Rac activity decreased rapidly. In a higher magnification, we noticed that Rac activity was highest immediately behind the leading edge (Fig. 4).

Cdc42 activity also increased toward the leading edge (Fig. 4). In the higher magnification, however, high Cdc42 activity is most concentrated at the tip of the leading edge (Fig. 4). In cells expressing Raichu-Rac-Y40C or Raichu-Cdc42-Y40C, we could not detect any gradient of the emission ratio, confirming that the intramolecular binding of CRIB to Rac or Cdc42 generated the gradient of FRET efficiency.

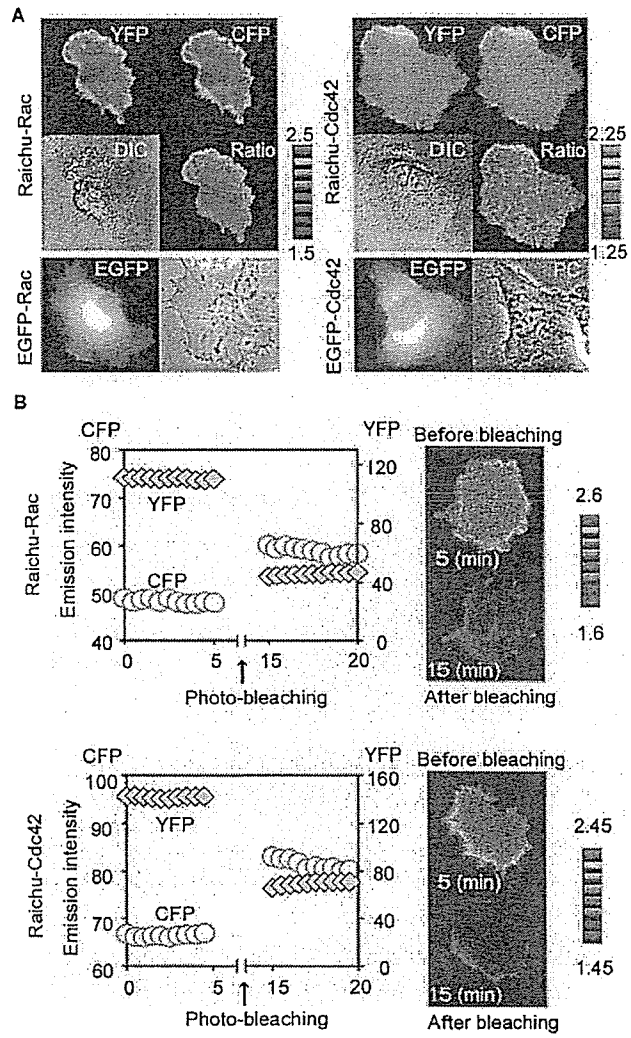


FIG. 3. Imaging of Rac and Cdc42 activities in HT1080 cells. (A) HT1080 cells were transfected with expression vectors as indicated on the left. After 48 h, cells expressing EGFP-Rac or EGFP-Cdc42 were photographed for EGFP and phase contrast (PC) images. Cells expressing Raichu-Rac or Raichu-Cdc42 were imaged for YFP, CFP, and differential interference contrast (DIC). In the IMD mode images (Ratio), eight colors from red to blue are used to represent the YFP/CFP ratio, with the intensity of each color indicating the mean intensity of YFP and CFP. The upper and lower limits of the ratio range are shown on the right. (B) Increase in the CFP emission by YFP photobleaching. HT1080 cells expressing Raichu-Rac or Raichu-Cdc42 were photobleached at an excitation wavelength of 510 nm for 10 min. Emission intensities of CFP and YFP in this cell were monitored every 30 s and are shown at the left. Cell images of pre- and postbleaching are shown at the right.

The activity of Ras was higher at the peripheral region, but there was no difference between the leading and the tailing edges. Rap1 activity was higher around the nucleus. Again, we could not observe a remarkable difference between the leading and the tailing edges, indicating that the gradual increase to-

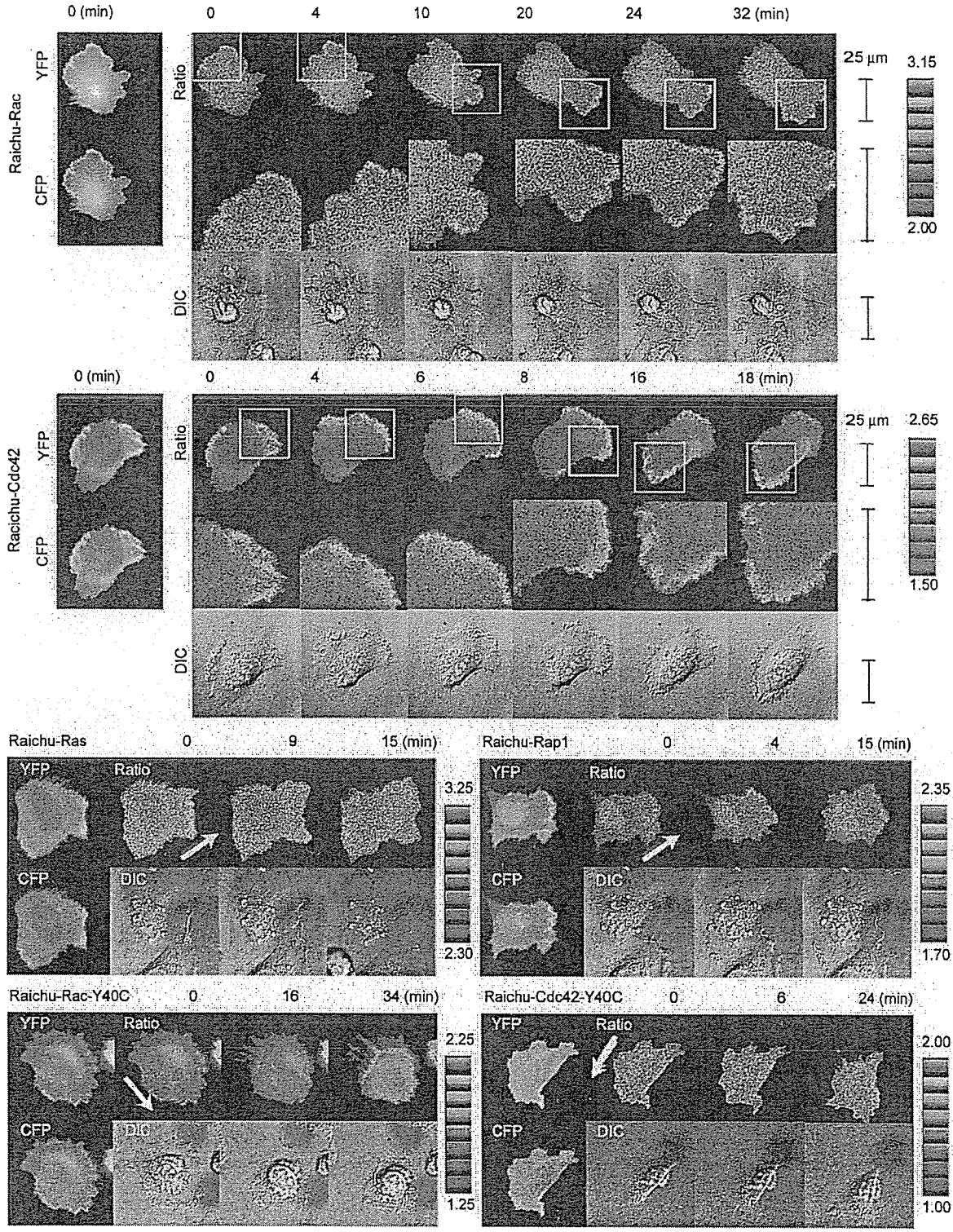


FIG. 4. Activity of Rac and Cdc42 in a motile HT1080 cell video imaged by using Raichu-Rac and Raichu-Cdc42. HT1080 cells infected with recombinant adenoviruses coding Raichu probes were replated onto a collagen-coated glass base dish. Beginning 1 h after replating, CFP, YFP, and differential interference contrast (DIC) images were obtained every 2 min with a time-lapse microscope. YFP/CFP ratio images were created to represent FRET efficiency, which correlated with the activities of the G proteins. Representative YFP, CFP, YFP/CFP (Ratio), and DIC images obtained at the indicated time points are shown. Arrows point in the direction of cell migration. The middle panels show magnified FRET images of the leading edges (boxes in the top panels). The upper and lower limits of the ratio range are shown on the right. The original video images are presented on our website (http://www-tv/biken.osaka-u.ac.jp/rei/). Experiments were performed at least five times for each probe, and similar results were obtained.

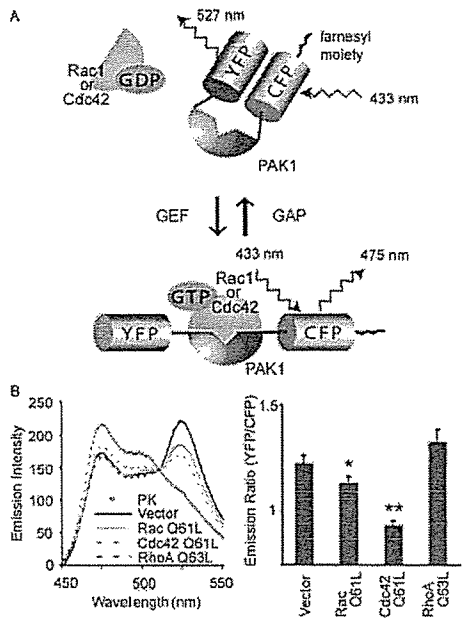


FIG. 5. Fluorescence profile of Raichu-CRIB. (A) Schematic representations of Raichu-CRIB and Raichu-CRIB-X with or without GTP-Rac or -Cdc42. The farnesyl moiety was fused only to Raichu-CRIB-X. When the probe is free, fluorescence at 527 nm by FRET is observed. When the probe is bound to GTP-Rac or GTP-Cdc42, YFP is displaced from CFP and FRET is inhibited. (B) 293T cells transfected with pRaichu-CRIB and pEB6-Rac1-Q61L, pEB6-Cdc42-Q61L, or pEB6-RhoA-Q63L were lysed and analyzed with a fluorescence spectrometer at an excitation wavelength of 433 nm (left). The lysates of the wild type were further treated with proteinase K (PK), which cleaved the probes between YFP and CFP. Mean YFP/CFP ratios are shown with standard error bars at the right. Single and double asterisks indicate that the differences between control and Rac1-Q61L and between control and Cdc42-Q61L, respectively, were statistically significant by $t$ test ($P < 0.05$ and $P < 0.01$, respectively).

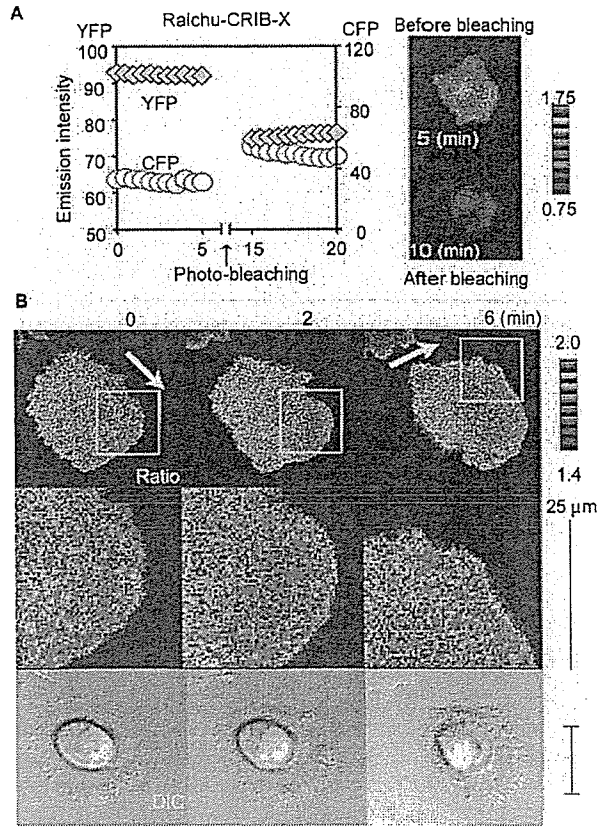


FIG. 6. Activity of Rac and Cdc42 video imaged with Raichu-CRIB-X. (A) Increase in the CFP emission by YFP photobleaching. HT1080 cells expressing Raichu-CRIB-X were photobleached at an excitation wavelength of 510 nm for 10 min. Emission intensities of CFP and YFP in these cells (left) were monitored every 30 s. Cell images of pre- and postbleaching are also shown (right). (B) HT1080 cells transfected with pRaichu-CRIB-X were replated onto a collagen-coated glass base dish. Beginning 1 h after replating, CFP, YFP, and differential interference contrast (DIC) images were obtained every 2 min with a time-lapse microscope as described in the legend to Fig. 4. Arrows point in the direction of cell migration. The upper and lower limits of the ratio range are shown on the right. The original video images are presented on our website (:http://www-tv/biken.osaka-u.ac.jp/rei/).

ward the leading edge was specific to the activities of Rac and Cdc42.

**Development of Raichu-CRIB.** RhoGDI recognizes the carboxy termini of geranyl-geranylated Rho family G proteins (10, 16). Because the carboxy terminus of Raichu-Rac and Raichu-Cdc42 consisted of the CAAX box of $K_i$-Ras, it was predictable that RhoGDI did not bind to Raichu-Rac or Raichu-Cdc42. Indeed, we did not observe the effect of overexpressed RhoGDI on the FRET efficiency of Raichu-Rac or Raichu-Cdc42 (data not shown). To compensate for this defect, we prepared another probe consisting of CRIB, YFP, and CFP as reported previously (Fig. 5A) (12). This probe, named Raichu-CRIB, was coexpressed with constitutively active Rac1, Cdc42, or RhoA in 293T cells. As shown in Fig. 5B, the FRET efficiency of Raichu-CRIB was decreased only in the presence of the active Rac1 or active Cdc42, not in the presence of the active RhoA. Therefore, in this Raichu-CRIB probe, the decrease in FRET indicated the binding to the active Cdc42 or Rac1. Notably, Rac1 decreased the FRET efficiency of Raichu-CRIB less efficiently than did Cdc42. This probably reflected the previous observation that the affinity of Rac1 for Pak is weaker than that of Cdc42 (52). The occurrence of FRET was confirmed by the proteinase K treatment as already described.

**Activities of Rac and Cdc42 monitored by Raichu-CRIB-X.** In HT1080 cells, Raichu-CRIB localized diffusely in the cytoplasm and there was no difference in its FRET efficiency throughout the cells (data not shown). We speculated that the excess of the probe and/or the limited binding to Rac and/or Cdc42 resulted in the failure to detect the Rac and Cdc42 activities. To increase the percentage of the probe that participated in the binding to Rac and Cdc42, the CAAX box of $K_i$-Ras was fused to the carboxy terminus of CFP, generating Raichu-CRIB-X (Fig. 5A). First, the occurrence of FRET in Raichu-CRIB-X-expressing cells was confirmed by a photobleaching experiment as already described. As expected, photobleaching of YFP resulted in a marked increase in the CFP intensity of the cells expressing Raichu-CRIB-X (Fig. 6A). Then, using Raichu-CRIB-X, we imaged the activities of Rac and Cdc42 in a motile HT1080 cell (Fig. 6B). We found that the FRET efficiency gradually decreased toward the leading

edge, indicating that the binding of CRIB to the endogenous Rac and/or Cdc42 gradually increased toward the leading edge. This observation was in complete agreement with findings obtained by using Raichu-Rac and Raichu-Cdc42 and also implied that RhoGDI did not contribute significantly to the spatial gradient of the Rac and Cdc42 activity in a motile HT1080 cell. Alternately, RhoGDI activity may have been cooperatively regulated with GEFs and GAPs to produce a gradient of Rac and Cdc42 activity.

**Analysis of GEF and GAP in 96-well plates with Raichu-Rac and Raichu-Cdc42.** We set up a rapid and simple cell-based assay for the measurement of GEF and GAP activities by the use of Raichu-Rac and Raichu-Cdc42. For this purpose, we removed the CAAX box from Raichu-Rac and Raichu-Cdc42, because CAAX-negative probes were expressed more abundantly in 293T cells than were CAAX-positive probes. To test the validity of our assay system, we obtained six putative GEFs and GAPs from the HUGE cDNA library of the Kazusa DNA Institute. As controls, we used Tiam-1, DOCK180, Vav, RasGRF1, and mSos-1, all of which contain the DH domain. The deduced domain structures of these GEFs and GAPs are shown schematically in Fig. 7A. The cDNAs were cotransfected with CAAX-negative pRaichu-Rac or pRaichu-Cdc42 into COS-1 cells, which were grown in glass bottom 96-well plates (Fig. 7B). The emission ratio of Raichu-Rac increased remarkably in the presence of Tiam-1 and DOCK180 and slightly in the presence of Vav and KIAA0362, demonstrating the GEF activity of these proteins toward Rac. GAP activity in response to Rac was detected only in KIAA0053. GEF activity in response to Cdc42 was detected in KIAA0362 and KIAA1256, and GAP activity in response to Cdc42 was detected in KIAA0053 and KIAA1204. Thus, we could examine the specificity of putative GEFs and GAPs by this simple method with Raichu probes.

**Dose response to GEFs and GAPs.** Finally, we confirmed the results obtained by the 96-well-plate-based assay with a fluorescence spectrometer. We expressed in 293T cells various quantities of DOCK180, KIAA0362/DBS, KIAA0053, and KIAA1204 with Raichu probes and examined the dose response. As shown in Fig. 7C, the FRET efficiency of Raichu-Rac increased with an increasing amount of DOCK180. Similarly, the FRET efficiency of Raichu-Cdc42 correlated with the amount of KIAA0362/DBS. In contrast, expression of KIAA0053 and KIAA1204 effectively decreased the emission ratio of Raichu-Rac and Raichu-Cdc42, respectively, in a dose-dependent manner.

## DISCUSSION

Probes based on the GFP and FRET technology have enormous potential for monitoring the intracellular signal transduction cascades in living cells (53). Nevertheless, the number of probes developed has not been increasing as might be expected. There are two problems to be overcome. When the assay system consists of two probes which are bound covalently to their respective donor and acceptor fluorophores, the relative amounts of the two probes cannot be controlled in most systems. Thus, bleed-through fluorescence, which emanates from the donor and which is detected in the acceptor channel, must be accurately compensated for in the estimation of FRET

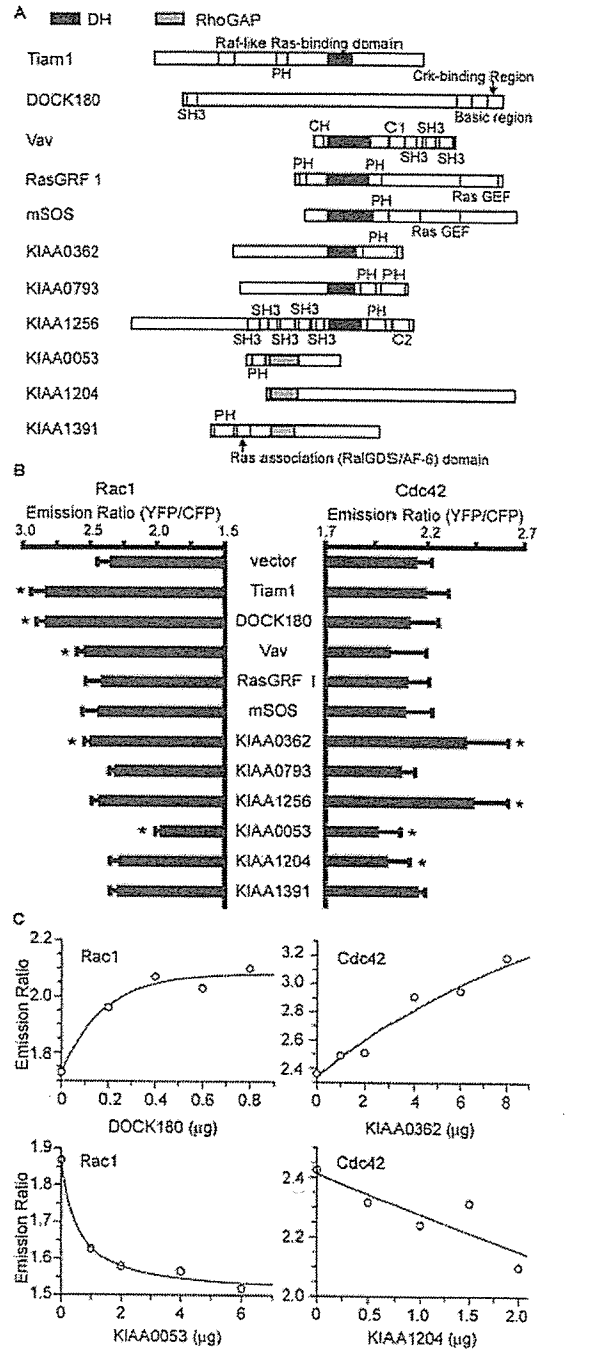


FIG. 7. Analysis of GEF and GAP activities. (A) Schematic representation of GEFs and GAPs used in this study. Abbreviations: PH, pleckstrin homology domain; DH, DH domain; SH2 and SH3, Src homology domains 2 and 3. (B) COS-1 cells plated on glass bottom 96-well plates were transfected with CAAX-negative pRaichu-Rac or pRaichu-Cdc42 and expression vectors for the proteins listed at the center. Cells were imaged, and the YFP/CFP ratio was determined as described in the text. Error bars, standard deviations. Asterisks, samples that show a difference from the control vector with statistical significance by $t$ test ($P < 0.01$). (C) CAAX-negative pRaichu-Rac or pRaichu-Cdc42 was coexpressed in 293T cells with various quantities of pCAGGS-DOCK180, pIRM21-KIAA0362/DBS, pIRM21-KIAA0053, and pIRM21-KIAA1204. Cells were lysed and examined for emission ratio as for Fig. 1B.

efficiency (2). A single-gene-encoded probe, in contrast, contains both the donor and acceptor; therefore, simply monitoring the ratio of donor fluorescence to acceptor fluorescence is sufficient. The problem with this type of probe resides in its construction. Typically, the probe is designed so that the signal-induced conformational change of the probe brings CFP into close proximity with YFP. The increases in FRET efficiency for most prototype probes, however, are less than 10% and do not apply to cell imaging. As for the first in vivo probe for Ras family G protein Raichu-Ras (36), where Ras is placed at the amino terminus of the Ras-binding domain of Raf, we originally placed Rac at the amino terminus of CRIB. In this construct, the difference in FRET efficiency between the wild-type and the G12V mutants was less than 10%. Only when we placed Rac or Cdc42 at the carboxy terminus of CRIB did we detect an increase in FRET in the G12V mutants. Thus, currently we cannot tell whether G proteins should be placed at the amino terminus or carboxy terminus of the binding partner in probe designs.

Rho family G proteins are regulated by three classes of proteins, GEF, GAP, and GDI. GDI controls the partitioning of the Rho family G proteins between the cytoplasm and cell membrane (43). By placing the probes constitutively at the membrane, the effect of GDI could not be monitored by Raichu-Rac and Raichu-Cdc42. Therefore, the activities of Rac and Cdc42 monitored by these probes are correctly expressed as the balance between GEF and GAP activities at the cell membrane. Although the regulatory role of GDI has been recently emerging (5, 50), it is widely accepted that many signaling cascades regulate Rac and Cdc42 by changing the balance of GEF and GAP activities at the cell membrane (51). Thus, Raichu-Rac and Raichu-Cdc42 provide useful tools to unravel the signaling cascades connected to Rac and Cdc42 pathways.

Irrespective of the loss of sensitivity to GDI, we fused the probes to the CAAX box of $K_i$-Ras for the following four reasons. First, active Rac and Cdc42 are detected only at the membrane compartments (43), providing a rationale for placing the probe only at the membrane. Second, we have found that an excess of cytosolic probes profoundly decreases the signal-to-noise ratio during the development of a probe for tyrosine phosphorylation (25). The same happened to Raichu-CRIB. To improve the signal-to-noise ratio, we needed to place Raichu-CRIB at the membrane. Third, CAAX-less probes diffuse throughout the cytoplasm within 10 s. Considering that the rate constants of most GEFs are between $10^{-3}$ and $10^{-2}$/s, we needed to restrict the movement of probes to obtain the spatial information (25). Last, we found that probes fused with the CAAX box of H-Ras or the myristylation signal of Src often accumulated at the Golgi apparatus, deteriorating the ratio image in the central region. In our hands, the CAAX box of $K_i$-Ras delivered the probes most uniformly to the membrane compartments.

We observed that the FRET efficiency of wild-type Raichu-Rac or Raichu-Cdc42 was remarkably higher than those of N17 and Y40C mutants (Fig. 1B) or than those in the presence of GAPs (Fig. 7B). This observation appears inconsistent with biochemical data. Because the GTP/GDP ratio of the wild-type Rac or Cdc42 was less than 10% in TLC analysis (Fig. 2), a further decrease in the GTP/GDP ratio of the wild-type Rac or Cdc42 should not significantly decrease their FRET efficiencies. This discrepancy probably reflects high GAP activity in the cell lysates, which results in the hydrolysis of GTP bound to Rac and Cdc42 during the immunoprecipitation before TLC analysis (3). Indeed, we observed that the FRET efficiency of the wild-type Raichu-Rac or Raichu-Cdc42 in the cell lysates decreased with time (data not shown).

It has been richly documented that Rac and Cdc42 induce lamellipodia and filopodia, respectively (51). Nevertheless, the mechanism underlying these unique morphological outputs remains elusive (51). Notably, both Rac and Cdc42 activate the two well-characterized signaling cascades that directly regulate actin polymerization, the PAK-LIM kinase-cofilin (49, 57) and N-WASP/WAVE-Arp2/3 (31, 46) pathways. Thus, it is likely that a difference in the distributions of active Rac and Cdc42 leads to distinct morphological changes. Indeed, such a possibility was supported by our observation that the activity of Rac was highest immediately behind the leading edge, whereas the Cdc42 activity was highest at the tip of the leading edge (Fig. 4). Moreover, this observation suggests that the leading-edge formation may be initiated by Cdc42 activation, followed by Rac activation. On the other hand, the gradual increase toward the leading edge is a feature common to Rac and Cdc42. This finding agrees with the presence of many GEFs and GAPs that act on both Rac and Cdc42 (51). In conclusion, our findings imply that both dual- and monospecific GEFs and GAPs contribute to the spatial regulation of Rac and Cdc42 in a motile HT1080 cell.

Raichu-Rac and Raichu-Cdc42 enabled us to rapidly identify the substrate specificity of putative GEFs and GAPs, the numbers of members of which have been expanding enormously with the progress of genome sequencing projects (51). For the demonstration of GEF or GAP activity in vitro, purified proteins are required; however, GEFs and GAPs are often insoluble in *Escherichia coli*. Alternately, to avoid their expression in *E. coli*, the putative GEFs or GAPs are expressed in mammalian cells and partially purified by immunoprecipitation for the in vitro analysis (3). In this case, preparation of a specific antibody or epitope tagging is required. We subcloned cDNAs of putative GEFs and GAPs into a eukaryotic expression vector using the same restriction enzymes that were employed for the construction of the KIAA cDNA libraries (38), minimizing the task of subcloning. The substrate specificities of the putative GEFs and GAPs were readily determined by coexpressing them with Raichu-Rac or Raichu-Cdc42 and examining FRET efficiency in COS-1 cells; no further manipulation was necessary. We are currently developing Raichu-Rho, a monitor for RhoA (H. Yoshizaki and M. Matsuda, unpublished data); therefore, the use of Raichu-Rho, Rac, and Cdc42 will cover the majority of Rho family G proteins and accelerate the characterization of GEFs and GAPs for the Rho family G proteins.

Among the three putative GEF proteins tested, KIAA0362 and KIAA1256 are found to be identical to DBS (54) and intersectin-2 (44), respectively. DBS/KIAA0362 has been shown to promote the guanine nucleotide exchange of RhoA and Cdc42 (55). Although GEF activity of intersectin-2/KIAA1256 has not been reported, a related protein, intersectin-1, has been demonstrated to be a GEF for Cdc42. Our observation is in agreement with these previous reports, except

that KIAA0362/DBS slightly stimulated Rac in our assay. This difference may be because we expressed the entire protein, whereas only the Dbl domain was used in the previous study (55). Alternately, this observation may simply reflect the fact that the substrate specificities of some GEFs and GAPs under in vitro conditions differ from those under and in vivo conditions. For instance, p50 RhoGAP stimulates GTPase activities of Rho, Rac, and Cdc42 in vitro but it stimulates only Rho in vivo (45).

Among the known activators of Rac or Cdc42 tested, we failed to detect the GEF activity of Ras-GRF1 and Sos-1. This observation probably reflects tight regulation of these GEFs in the cells. Ras-GRF1 is activated only in the presence of the $\beta\gamma$ subunit or by phosphorylation (21, 22). Similarly, Rac GEF activity of Sos-1 requires phosphatidylinositol 3-kinase activation (39). Therefore, the assay system with Raichu-Rac or Raichu-Cdc42 appears to reflect the in vivo enzyme activity of GEFs and GAPs. This property will enable us to study the regulatory mechanism of GEFs and GAPs in living cells by a simple imaging technique with Raichu-Rac and Raichu-Cdc42.

Finally, it should be remembered that every monitoring system for Rho family G proteins has some defects. For example, due to the high GAP activity in the cell lysates, the GTP/GDP ratios of the authentic Rac and Cdc42 are barely measurable by the classical TLC analysis (3, 20). As a simple and safer alternative, Bos's pull-down method has been applied to detect the activation of Rac and Cdc42 in cells (6, 23); however, none has ever shown that the activity detected by this method correlates with the increases in the GTP/GDP ratios of Rac and Cdc42 in the cells. Considering the inefficient recovery rate of the GTP-bound form (19), the results obtained by the pull-down method have to be interpreted with careful attention. Raichu-Rac and Raichu-Cdc42 also suffer from the defect that they cannot monitor RhoGDI activity. Raichu-CRIB complements this defect, but possesses the flaw that it may competitively interfere the endogenous Rac and Cdc42 signaling cascades. Indeed, we found that overexpression of Raichu-CRIB was apparently toxic to the cells. Another demerit of Raichu-CRIB is its reactivity with both Rac and Cdc42, rendering the interpretation of the data complicated. Thus, Raichu-CRIB may be used as an auxiliary method for Raichu-Rac and Raichu-Cdc42 to evaluate the effect of RhoGDI.

In conclusion, because none of the other methods can currently obtain spatiotemporal information on Rac and Cdc42 activity in living cells, the FRET-based probes reported in this study will accelerate research to delineate the spatiotemporal regulation of Rac and Cdc42 in living cells.

## ACKNOWLEDGMENTS

We thank A. Miyawaki, Y. Takai, H. Mano, J. M. Adams, J. Collard, S. Hattori, L. Feig, J. Miyazaki, and B. J. Mayer for plasmids and N. Fujimoto, N. Yoshida, and Y. Matsuura for technical assistance.

This work was supported in part by grants from the Ministry of Education, Science, Sports and Culture, the Ministry of Health and Welfare, and the Health Science Foundation of Japan.

## REFERENCES

1. **Bar-Sagi, D., and A. Hall.** 2000. Ras and Rho GTPases: a family reunion. Cell **103**:227–238.
2. **Chamberlain, C. E., V. S. Kraynov, and K. M. Hahn.** 2000. Imaging spatiotemporal dynamics of Rac activation in vivo with FLAIR. Methods Enzymol. **325**:389–400.
3. **Crespo, P., K. E. Schuebel, A. A. Ostrom, J. S. Gutkind, and X. R. Bustelo.** 1997. Phosphotyrosine-dependent activation of Rac-1 GDP/GTP exchange by the vav proto-oncogene product. Nature **385**:169–172.
4. **Day, R. N.** 1998. Visualization of Pit-1 transcription factor interactions in the living cell nucleus by fluorescence resonance energy transfer microscopy. Mol. Endocrinol. **12**:1410–1419.
5. **del Pozo, M. A., W. B. Kiosses, N. B. Alderson, N. Meller, K. M. Hahn, and M. A. Schwartz.** 2002. Integrins regulate GTP-Rac localized effector interactions through dissociation of Rho-GDI. Nat. Cell Biol. **4**:232–239.
6. **del Pozo, M. A., L. S. Price, N. B. Alderson, X. D. Ren, and M. A. Schwartz.** 2000. Adhesion to the extracellular matrix regulates the coupling of the small GTPase Rac to its effector PAK. EMBO J. **19**:2008–2014.
7. **Feig, L. A., and G. M. Cooper.** 1988. Inhibition of NIH3T3 cell proliferation by a mutant ras protein with preferential affinity for GDP. Mol. Cell. Biol. **8**:3235–3243.
8. **Fradkov, A. F., Y. Chen, L. Ding, E. V. Barsova, M. V. Matz, and S. A. Lukyanov.** 2000. Novel fluorescent protein from Discosoma coral and its mutants possesses a unique far-red fluorescence. FEBS Lett. **479**:127–130.
9. **Geiger, B., and A. Bershadsky.** 2001. Assembly and mechanosensory function of focal contacts. Curr. Opin. Cell Biol. **13**:584–592.
10. **Gosser, Y. Q., T. K. Nomanbhoy, B. Aghazadeh, D. Manor, C. Combs, R. A. Cerione, and M. K. Rosen.** 1997. C-terminal binding domain of Rho GDP-dissociation inhibitor directs N-terminal inhibitory peptide to GTPases. Nature **387**:814–819.
11. **Gotoh, T., Y. Niino, M. Tokuda, O. Hatase, S. Nakamura, M. Matsuda, and S. Hattori.** 1997. Activation of R-Ras by ras-guanine nucleotide-releasing factor. J. Biol. Chem. **272**:18602–18607.
12. **Graham, D. L., P. N. Lowe, and P. A. Chalk.** 2001. A method to measure the interaction of Rac/Cdc42 with their binding partners using fluorescence resonance energy transfer between mutants of green fluorescent protein. Anal. Biochem. **296**:208–217.
13. **Hall, A., and C. D. Nobes.** 2000. Rho GTPases: molecular switches that control the organization and dynamics of the actin cytoskeleton. Phil. Trans. R. Soc. Lond. B Biol. Sci. **355**:965–970.
14. **Hasegawa, H., E. Kiyokawa, S. Tanaka, K. Nagashima, N. Gotoh, M. Shibuya, T. Kurata, and M. Matsuda.** 1996. DOCK180, a major CRK-binding protein, alters cell morphology upon translocation to the membrane. Mol. Cell. Biol. **16**:1770–1776.
15. **Heim, R., and R. Y. Tsien.** 1996. Engineering green fluorescent protein for improved brightness, longer wavelengths and fluorescence resonance energy transfer. Curr. Biol. **6**:178–182.
16. **Hoffman, G. R., N. Nassar, and R. A. Cerione.** 2000. Structure of the Rho family GTP-binding protein Cdc42 in complex with the multifunctional regulator RhoGDI. Cell **100**:345–356.
17. **Kanegae, Y., G. Lee, Y. Sato, M. Tanaka, M. Nakai, T. Sakaki, S. Sugano, and I. Saito.** 1995. Efficient gene activation in mammalian cells by using recombinant adenovirus expressing site-specific Cre recombinase. Nucleic Acids Res. **23**:3816–3821.
18. **Katzav, S., D. Martin-Zanca, and M. Barbacid.** 1989. vav, a novel human oncogene derived from a locus ubiquitously expressed in hematopoietic cells. EMBO J. **8**:2283–2290.
19. **Kimura, K., T. Tsuji, Y. Takada, T. Miki, and S. Narumiya.** 2000. Accumulation of GTP-bound RhoA during cytokinesis and a critical role of ECT2 in this accumulation. J. Biol. Chem. **275**:17233–17236.
20. **Kiyokawa, E., Y. Hashimoto, S. Kobayashi, H. Sugimura, T. Kurata, and M. Matsuda.** 1998. Activation of Rac1 by a Crk SH3-binding protein, DOCK180. Genes Dev. **12**:3331–3336.
21. **Kiyono, M., Y. Kaziro, and T. Satoh.** 2000. Induction of rac-guanine nucleotide exchange activity of Ras-GRF1/CDC25(Mm) following phosphorylation by the nonreceptor tyrosine kinase Src. J. Biol. Chem. **275**:5441–5446.
22. **Kiyono, M., T. Satoh, and Y. Kaziro.** 1999. G protein betagamma subunit-dependent rac-guanine nucleotide exchange activity of ras-GRF1/CDC25(Mm). Proc. Natl. Acad. Sci. USA **96**:4826–4831.
23. **Kobayashi, S., T. Shirai, E. Kiyokawa, N. Mochizuki, M. Matsuda, and Y. Fukui.** 2001. Membrane recruitment of DOCK180 by binding to PtdIns(3,4,5,)$P_3$. Biochem. J. **354**:73–78.
24. **Kraynov, V. S., C. Chamberlain, G. M. Bokoch, M. A. Schwartz, S. Slabaugh, and K. M. Hahn.** 2000. Localized rac activation dynamics visualized in living cells. Science **290**:333–337.
25. **Kurokawa, K., N. Mochizuki, Y. Ohba, H. Mizuno, A. Miyawaki, and M. Matsuda.** 2001. A pair of FRET-based probes for tyrosine phosphorylation of the CrkII adapter protein in vivo. J. Biol. Chem. **276**:31305–31310.
26. **Lamarche, N., N. Tapon, L. Stowers, P. D. Burbelo, P. Aspenstrom, T. Bridges, J. Chant, and A. Hall.** 1996. Rac and Cdc42 induce actin polymerization and $G_1$ cell cycle progression independently of p65(PAK) and the JNK/SAPK MAP kinase cascade. Cell **87**:519–529.
27. **Mahajan, N. P., D. C. Harrison-Shostak, J. Michaux, and B. Herman.** 1999. Novel mutant green fluorescent protein protease substrates reveal the activation of specific caspases during apoptosis. Chem. Biol. **6**:401–409.
28. **Mahajan, N. P., K. Linder, G. Berry, G. W. Gordon, R. Heim, and B. Herman.** 1998. Bcl-2 and Bax interactions in mitochondria probed with

green fluorescent protein and fluorescence resonance energy transfer. Nat. Biotechnol. 16:547–552.
29. Matsuda, M., Y. Hashimoto, K. Muroya, H. Hasegawa, T. Kurata, S. Tanaka, S. Nakamura, and S. Hattori. 1994. CRK binds to two guanine nucleotide-releasing proteins for the Ras family and modulates nerve growth factor-induced activation of Ras in PC12 cells. Mol. Cell. Biol. 14:5495–5500.
30. Michiels, F., G. G. Habets, J. C. Stam, R. A. van der Kammen, and J. G. Collard. 1995. A role for Rac in Tiam1-induced membrane ruffling and invasion. Nature 375:338–340.
31. Miki, H., T. Sasaki, Y. Takai, and T. Takenawa. 1998. Induction of filopodium formation by a WASP-related actin-depolymerizing protein N-WASP. Nature 391:93–96.
32. Miki, T. 1995. Interaction of ect2 and Dbl with Rho-related GTPases. Methods Enzymol. 256:90–98.
33. Mitra, R. D., C. M. Silva, and D. C. Youvan. 1996. Fluorescence resonance energy transfer between blue-emitting and red-shifted excitation derivatives of the green fluorescent protein. Gene 173:13–17.
34. Miyawaki, A., J. Llopis, R. Heim, J. M. McCaffery, J. A. Adams, M. Ikura, and R. Y. Tsien. 1997. Fluorescent indicators for Ca2+ based on green fluorescent proteins and calmodulin. Nature 388:882–887.
35. Mizuno, H., A. Sawano, P. Eli, H. Hama, and A. Miyawaki. 2001. Red fluorescent protein from Discosoma as a fusion tag and a partner for fluorescence resonance energy transfer. Biochemistry 40:2502–2510.
36. Mochizuki, N., S. Yamashita, K. Kurokawa, Y. Ohba, T. Nagai, A. Miyawaki, and M. Matsuda. 2001. Spacio-temporal images of growth factor-induced activation of Ras and Rap1. Nature 411:1065–1068.
37. Nagai, Y., M. Miyazaki, R. Aoki, T. Zama, S. Inouye, K. Hirose, M. Iino, and M. Hagiwara. 2000. A fluorescent indicator for visualizing cAMP-induced phosphorylation in vivo. Nat. Biotechnol. 18:313–316.
38. Nagase, T., N. Seki, K. Ishikawa, M. Ohira, Y. Kawarabayasi, O. Ohara, A. Tanaka, H. Kotani, N. Miyajima, and N. Nomura. 1996. Prediction of the coding sequences of unidentified human genes. VI. The coding sequences of 80 new genes (KIAA0201-KIAA0280) deduced by analysis of cDNA clones from cell line KG-1 and brain. DNA Res. 3:321–354.
39. Nimnual, A. S., B. A. Yatsula, and D. Bar-Sagi. 1998. Coupling of Ras and Rac guanosine triphosphatases through the Ras exchanger Sos. Science 279:560–563.
40. Niwa, H., K. Yamamura, and J. Miyazaki. 1991. Efficient selection for high-expression transfectants with a novel eukaryotic vector. Gene 108:193–200.
41. Nobes, C. D., and A. Hall. 1995. Rho, rac, and cdc42 GTPases regulate the assembly of multimolecular focal complexes associated with actin stress fibers, lamellipodia, and filopodia. Cell 81:53–62.
42. Ohba, Y., N. Mochizuki, K. Matsuo, S. Yamashita, M. Nakaya, Y. Hashimoto, M. Hamaguchi, T. Kurata, K. Nagashima, and M. Matsuda. 2000. Rap2 as a slowly responding molecular switch in the Rap1 signaling cascade. Mol. Cell. Biol. 20:6074–6083.
43. Olofsson, B. 1999. Rho guanine dissociation inhibitors: pivotal molecules in cellular signalling. Cell Signal. 11:545–554.
44. Pucharcos, C., C. Casas, M. Nadal, X. Estivill, and S. de la Luna. 2001. The human intersectin genes and their spliced variants are differentially expressed. Biochim. Biophys. Acta 1521:1–11.
45. Ridley, A. J., A. J. Self, F. Kasmi, H. F. Paterson, A. Hall, C. J. Marshall, and C. Ellis. 1993. rho family GTPase activating proteins p190, bcr and rhoGAP show distinct specificities in vitro and in vivo. EMBO J. 12:5151–5160.
46. Rohatgi, R., L. Ma, H. Miki, M. Lopez, T. Kirchhausen, T. Takenawa, and M. W. Kirschner. 1999. The interaction between N-WASP and the Arp2/3 complex links Cdc42-dependent signals to actin assembly. Cell 97:221–231.
47. Romoser, V. A., P. M. Hinkle, and A. Persechini. 1997. Detection in living cells of $Ca^{2+}$-dependent changes in the fluorescence emission of an indicator composed of two green fluorescent protein variants linked by a calmodulin-binding sequence. A new class of fluorescent indicators. J. Biol. Chem. 272:13270–13274.
48. Sastry, S. K., and K. Burridge. 2000. Focal adhesions: a nexus for intracellular signaling and cytoskeletal dynamics. Exp. Cell Res. 261:25–36.
49. Sumi, T., K. Matsumoto, Y. Takai, and T. Nakamura. 1999. Cofilin phosphorylation and actin cytoskeletal dynamics regulated by Rho- and Cdc42-activated LIM-kinase 2. J. Cell Biol. 147:1519–1532.
50. Takahashi, K., T. Sasaki, A. Mammoto, K. Takaishi, T. Kameyama, S. Tsukita, and Y. Takai. 1997. Direct interaction of the Rho GDP dissociation inhibitor with ezrin/radixin/moesin initiates the activation of the Rho small G protein. J. Biol. Chem. 272:23371–23375.
51. Takai, Y., T. Sasaki, and T. Matozaki. 2001. Small GTP-binding proteins. Physiol Rev. 81:153–208.
52. Thompson, G., D. Owen, P. A. Chalk, and P. N. Lowe. 1998. Delineation of the Cdc42/Rac-binding domain of p21-activated kinase. Biochemistry 37: 7885–7891.
53. Tsien, R. Y., and A. Miyawaki. 1998. Seeing the machinery of live cells. Science 280:1954–1955.
54. Whitehead, I., H. Kirk, and R. Kay. 1995. Retroviral transduction and oncogenic selection of a cDNA encoding Dbs, a homolog of the Dbl guanine nucleotide exchange factor. Oncogene 10:713–721.
55. Whitehead, I. P., Q. T. Lambert, J. A. Glaven, K. Abe, K. L. Rossman, G. M. Mahon, J. M. Trzaskos, R. Kay, S. L. Campbell, and C. J. Der. 1999. Dependence of Dbl and Dbs transformation on MEK and NF-κB activation. Mol. Cell. Biol. 19:7759–7770.
56. Xu, X., A. L. V. Gerard, B. C. Huang, D. C. Anderson, D. G. Payan, and Y. Luo. 1998. Detection of programmed cell death using fluorescence energy transfer. Nucleic Acids Res. 26:2034–2035.
57. Yang, N., O. Higuchi, K. Ohashi, K. Nagata, A. Wada, K. Kangawa, E. Nishida, and K. Mizuno. 1998. Cofilin phosphorylation by LIM-kinase 1 and its role in Rac-mediated actin reorganization. Nature 393:809–812.

ELSEVIER

Autonomic Neuroscience: Basic and Clinical 95 (2002) 37–42

AUTONOMIC NEUROSCIENCE: Basic & Clinical

www.elsevier.com/locate/autneu

# Effects of brief ischaemia on myocardial acetylcholine and noradrenaline levels in anaesthetized cats

Toru Kawada [a,*], Toji Yamazaki [b], Tsuyoshi Akiyama [b], Hidezo Mori [b], Masashi Inagaki [a], Toshiaki Shishido [a], Hiroshi Takaki [a], Masaru Sugimachi [a], Kenji Sunagawa [a]

[a] *Department of Cardiovascular Dynamics, National Cardiovascular Center Research Institute, 5-7-1 Fujishirodai, Suita, Osaka 565-8565, Japan*
[b] *Department of Cardiac Physiology, National Cardiovascular Center Research Institute, 5-7-1 Fujishirodai, Suita, Osaka 565-8565, Japan*

Received 4 May 2001; received in revised form 29 July 2001; accepted 19 September 2001

**Abstract**

Although brief ischaemic events make the myocardium tolerant to subsequent prolonged ischaemia, known as ischaemic preconditioning, whether brief ischaemia also affects neural regulation at the in vivo heart remains unknown. We examined the effects of brief ischaemia on myocardial interstitial acetylcholine (ACh) and noradrenaline (NA) levels in anaesthetized cats ($n=6$). Baseline ACh and NA levels were $0.65 \pm 0.13$ and $0.66 \pm 0.17$ nmol $l^{-1}$ (mean ± SE), respectively. Two sets of 5-min brief occlusion followed by 20-min reperfusion of the left anterior descending coronary artery (LAD) significantly increased the myocardial interstitial ACh level to $4.6 \pm 0.7$ nmol $l^{-1}$ ($P<0.01$), while not affecting the myocardial interstitial NA level. Subsequent 60-min LAD occlusion significantly increased the ACh and NA levels to $34.9 \pm 6.0$ and $96.5 \pm 17.0$ nmol $l^{-1}$ ($P<0.01$), respectively. Vagotomy abolished the myocardial interstitial ACh release during brief ischaemia and attenuated the ACh release during subsequent 60-min ischaemia ($n=6$). In contrast, vagotomy did not affect the subsequent ischaemia-induced myocardial interstitial NA release. We conclude that the brief ischaemia affects myocardial interstitial ACh release but not NA release in the ischaemic myocardium in vivo. 

*Keywords:* Cardiac microdialysis; Vagotomy; Coronary artery occlusion; Ischaemic preconditioning

## 1. Introduction

Brief ischaemic events make the myocardium tolerant to subsequent more severe ischaemia. This phenomenon is termed ischaemic preconditioning (Murry et al., 1986; Reimer and Jennings, 1992). Recent investigations revealed that the ischaemic preconditioning is not limited to the heart, and is observed in other organ systems including the central nervous system (Dawson and Dawson, 2000). However, whether brief ischaemia affects neural regulation at the in vivo heart remains unknown. Because neurotransmitters directly act on the myocardium, elucidating the effects of brief ischaemia on neurotransmitter release in the ischaemic myocardium would be important for better understanding the neural control of the heart associated with ischaemic heart diseases.

With respect to the sympathetic system, Seyfarth et al. (1996) reported that transient ischaemia reduces noradrenaline (NA) release during subsequent prolonged ischaemia in the isolated rat heart perfused by modified Krebs–Henseleit solution. However, whether brief ischaemia affects myocardial interstitial NA release in vivo remains undetermined. With respect to the vagal system, few studies reported ischaemia-induced myocardial interstitial acetylcholine (ACh) release. In a previous study, we demonstrated that 60-min myocardial ischaemia increased myocardial interstitial ACh and NA levels in the ischaemic myocardium in anaesthetized cats (Kawada et al., 2000). In the present study, we focused on the effects of brief ischaemia on the sustained ischaemia-induced myocardial interstitial ACh and NA release. Furthermore, the effects of brief ischaemia were compared between animals with and without vagotomy. We made use of a cardiac microdialysis technique to measure myocardial interstitial ACh and NA levels (Akiyama et al., 1991, 1994; Kawada et al., 1999, 2000, 2001a,b; Yamazaki et al., 1997, 1998, 1999).

* Corresponding author. Tel.: +81-6-6833-5012x2427; fax: +81-6-6835-5403.
*E-mail address:* torukawa@res.ncvc.go.jp (T. Kawada).

1566-0702/02/$ - see front matter 
PII: S1566-0702(01)00352-6

## 2. Materials and methods

### 2.1. Animal preparation

Animal care was conducted in accordance with the *Guiding Principles for the Care and Use of Animals in the Field of Physiological Sciences* approved by the Physiological Society of Japan. Adult cats weighing 2.5–5.0 kg (3.7 ± 0.8 kg, mean ± SD) were anaesthetized via an intraperitoneal injection of pentobarbital sodium (30–35 mg/kg) and ventilated mechanically with room air mixed with oxygen. The depth of anaesthesia was maintained with a continuous intravenous infusion of pentobarbital sodium (1–2 mg/kg/h) through a catheter inserted from the right femoral vein. Mean arterial pressure (MAP) was measured from a catheter inserted from the right femoral artery. Heart rate (HR) was recorded through an electrocardiogram. When vagotomy was required, bilateral vagi were sectioned at the neck.

With the animal in the lateral position, the left fifth and sixth ribs were partially resected to expose the heart. A 4–0 silk suture was passed around the left anterior descending coronary artery (LAD) just distal to the first diagonal branch, and both of its ends were passed through a polyethylene tube to make a snare for later LAD occlusion. With a fine guiding needle, a dialysis probe was implanted into the anterolateral free wall of the left ventricle perfused by LAD to measure myocardial interstitial ACh and NA levels in the ischaemic region. Judging from changes in colour of the ventricular wall during sustained ischaemia, the dialysis probe was located in the midst of the ischaemic area. Heparin sodium (100 U/kg) was administered intravenously to prevent blood coagulation.

Each experimental animal was killed by an overdose of intravenous pentobarbital sodium at the end of the experiment. We performed a postmortem examination and confirmed that the dialysis probe had been implanted within the left ventricular myocardium.

### 2.2. Dialysis technique

We measured ACh and NA concentrations in the dialysate as indices of myocardial interstitial ACh and NA levels, respectively. The materials and properties of the dialysis probe have been previously described (Akiyama et al., 1991, 1994). Briefly, we designed a transverse dialysis probe. A dialysis fiber (13 mm length, 310 μm O.D., 200 μm I.D.; PAN-1200, 50,000 molecular weight cutoff, Asahi Chemical, Japan) was glued at both ends to polyethylene tubes (25 cm length, 500 μm O.D., 200 μm I.D.). The dialysis probe was perfused at a rate of 2 $\mu l \cdot min^{-1}$ with Ringer solution containing a cholinesterase inhibitor, eserine (100 μM). Dialysate samples were collected from 2 h after implantation of the dialysis probe (Akiyama et al., 1991). A single sampling period was set to be 15 min long, yielding a sample volume of 30 μl. Each sample was collected in a microtube containing 3 μl of phosphate buffer (0.1 M, pH 3.5) to prevent amine oxidation. The actual dialysate sampling lagged behind a given collection period by 5 min, taking into account the dead space volume between the semipermeable membrane and the sample microtube.

Two-thirds of the dialysate sample were used for the ACh measurement, and the remaining for the NA measurement. The ACh concentration in the dialysate was measured directly by high performance liquid chromatography with electrochemical detection (HPLC-ECD) (Eicom, Japan). The NA concentration in the dialysate was measured by another HPLC-ECD after the removal of interfering compounds by an alumina procedure. Details of HPLC-ECD for the ACh and NA measurements have been previously described (Akiyama et al., 1991, 1994).

### 2.3. Experimental protocols

We performed two sets of 5-min brief occlusion followed by 20-min reperfusion of LAD, and then occluded LAD for 60 min (Fig. 1). Finally, we reperfused LAD for 15 min. The 15-min dialysate samples were collected during control (C), brief ischaemia ($B_1$ and $B_2$), sustained ischaemia ($S_1$, $S_2$, $S_3$ and $S_4$), and the final reperfusion (R). We performed this protocol in animals with intact vagi (INT-BI, $n=6$) or vagotomy (VX-BI, $n=6$).

In a previous paper, we performed the 60-min LAD occlusion without preceding brief ischaemia in animals with intact vagi (INT, $n=7$) or vagotomy (VX, $n=6$) (Kawada et al., 2000). Although the complete time courses of the ACh and NA responses in the INT and VX groups have already been reported, for convenience, the ACh and NA levels during the last 15 min of the 60-min LAD occlusion are included in the present paper (as Fig. 4) to compare the results with the INT-BI and VX-BI groups. The experimental procedure and settings were consistent between the previous and present studies.

### 2.4. Statistics

All data are presented as mean ± SE values. In the INT-BI and VX-BI groups, we examined the difference in the ACh and NA levels against respective control values by

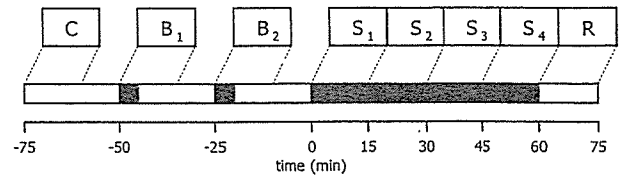


Fig. 1. Protocol for brief ischaemia and subsequent ischaemia. Black bars indicate the occlusion periods of left anterior descending coronary artery. Fifteen-minute dialysate samples were collected under conditions of control (C), brief ischaemia ($B_1$, $B_2$), subsequent sustained ischaemia ($S_1$, $S_2$, $S_3$, $S_4$), and reperfusion (R).

nonparametric Dunnett's test based on ranks following Friedman's test statistics (Glantz, 1997). Because changes in NA levels during 60-min myocardial ischaemia reached some 100 times the control level (Kawada et al., 2000), a normal distribution of the data necessary for a parametric test could not be assumed. Differences from respective control values were considered significant when $P<0.05$.

In relation to HR and MAP data, we used parametric Dunnett's test following repeated-measures multiple comparison (Glantz, 1997), as we could assume normal distributions for these data. Differences from respective control values were considered significant when $P<0.05$.

We examined differences in the ACh and NA responses during the last 15 min of the 60-min LAD occlusion among the INT, VX, INT-BI, and VX-BI groups using nonparametric Dunn's test based on ranks following Kruskal–Wallis test statistics (Glantz, 1997). While Dunnett's test is designed for repeated-measures multiple comparison (each subject receives more than one treatment), Dunn's test is designed for experiments in which each group contains different individuals. Differences from the INT group were considered significant when $P<0.05$.

## 3. Results

Changes in the myocardial interstitial ACh levels in the INT-BI and VX-BI groups are shown in Fig. 2. The brief ischaemia significantly increased the ACh level in the INT-BI group to about five times the control value. In contrast, the brief ischaemia did not increase the ACh level in the VX-BI group. The 60-min sustained ischaemia significantly increased the ACh level above the control value in both the INT-BI and VX-BI groups. The final reperfusion decreased the ACh level toward the control value in both groups.

Changes in the myocardial interstitial NA levels in the INT-BI and VX-BI groups are shown in Fig. 3. The inset illustrates the enlarged ordinate for the NA response to the brief ischaemia. The brief ischaemia altered the NA level in neither the INT-BI nor VX-BI group. The 60-min sustained ischaemia significantly increased the NA level above the control value in both the INT-BI and VX-BI groups except for the first 15 min. The final reperfusion decreased the NA level toward the control value in both groups.

Myocardial interstitial ACh levels during the last 15 min of the 60-min sustained ischaemia for the INT, VX, INT-BI and VX-BI groups are summarized in Fig. 4A. The INT-BI

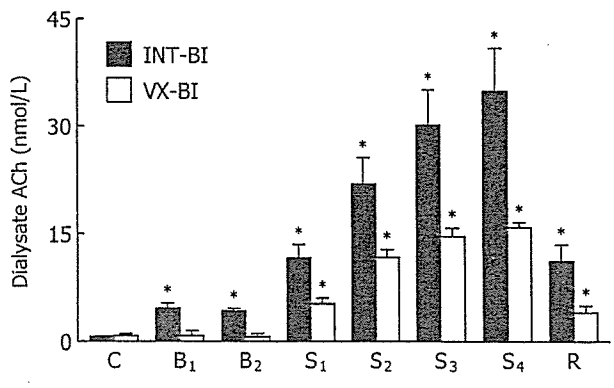


Fig. 2. Changes in myocardial acetylcholine (ACh) levels during brief ischaemia and subsequent sustained ischaemia in animals with intact vagi (INT-BI) or vagotomy (VX-BI). Data are means ± SE. *$P<0.01$ against control.

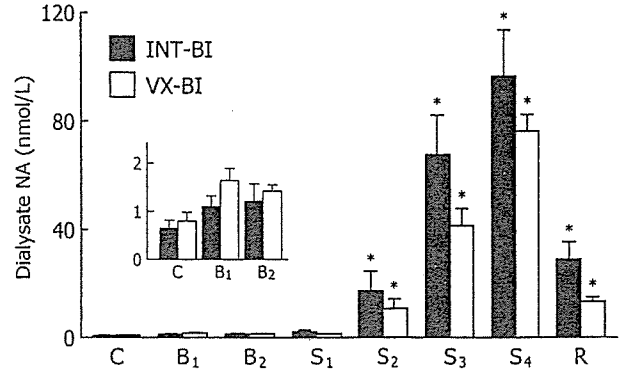


Fig. 3. Changes in myocardial noradrenaline (NA) levels during brief ischaemia and subsequent sustained ischaemia in animals with intact vagi (INT-BI) or vagotomy (VX-BI). Data are means ± SE. *$P<0.01$ against control.

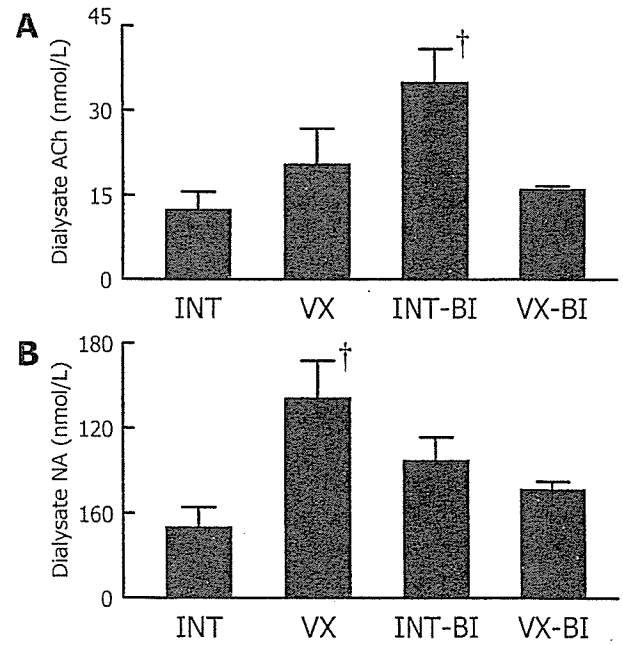


Fig. 4. (A) Ischaemia-induced acetylcholine (ACh) responses during the last 15 min of 60-min left anterior coronary artery occlusion. (B) Ischaemia-induced noradrenaline (NA) responses during the last 15 min of 60-min left anterior coronary artery occlusion. INT: intact vagi without preceding brief ischaemia, VX: vagotomy without preceding brief ischaemia, INT-BI: intact vagi with preceding brief ischaemia, VX-BI: vagotomy with preceding brief ischaemia. Data are means ± SE. †$P<0.05$ compared with the INT group.

Table 1
Changes in heart rate (HR) and mean arterial pressure (MAP) in INT-BI group

| | C | $B_1$ | $B_2$ | $S_1$ | $S_2$ | $S_3$ | $S_4$ | R |
|---|---|---|---|---|---|---|---|---|
| HR (beats/min) | 177.5 ± 9.9 | 160.5 ± 8.0 | 159.0 ± 6.5 | 162.8 ± 7.2 | 162.2 ± 7.7 | 159.2 ± 9.1 | 162.5 ± 8.7 | 161.3 ± 7.3 |
| MAP (mm Hg) | 115.7 ± 6.4 | 94.8 ± 8.1[a] | 101.2 ± 8.5[b] | 105.0 ± 7.9 | 95.8 ± 9.3[a] | 97.7 ± 9.8[a] | 93.3 ± 8.6[a] | 93.0 ± 8.2[a] |

Values are means ± SEM.
Data were obtained during control (C), after 5 min of each brief ischaemia ($B_1$ and $B_2$), after 5, 30, 45 and 60 min of sustained ischaemia ($S_1$, $S_2$, $S_3$ and $S_4$), and after 5 min of reperfusion (R).
[a] $P<0.01$ from control.
[b] $P<0.05$ from control.

group demonstrated a significantly greater ACh response than the INT group, whereas the VX and VX-BI groups showed the ACh responses similar to the INT group. Myocardial interstitial NA levels during the last 15 min of the 60-min sustained ischaemia for the four groups are summarized in Fig. 4B. In contrast to the ACh response, the VX group showed a significantly greater NA response than the INT group. The INT-BI and VX-BI groups did not show significant difference in the NA level as compared with the INT group.

Changes in HR and MAP in the INT-BI group are summarized in Table 1. HR did not change significantly throughout the protocol. MAP decreased during brief ischaemia and after 30 min of the sustained ischaemia. Changes in HR and MAP obtained from the VX-BI group are shown in Table 2. HR did not change significantly throughout the protocol. MAP decreased after 30 min of the sustained ischaemia.

## 4. Discussion

### *4.1. Effects of brief ischaemia on myocardial interstitial ACh and NA levels*

To our best knowledge, this is the first to demonstrate that 5-min brief ischaemia significantly increased myocardial interstitial ACh levels (Fig. 2, INT-BI). The ACh levels were similar in the first and second events of brief ischaemia ($B_1$ and $B_2$), suggesting that the cumulative effect of brief ischaemia on the ACh release was negligible in the present protocol. In contrast to the INT-BI group, brief ischaemia did not increase the myocardial interstitial ACh level in the VX-BI group (Fig. 2, VX-BI). Therefore, the myocardial interstitial ACh release during brief ischaemia is dependent upon intact vagal innervation. Mechanical or chemical stimulation during myocardial ischaemia evokes cardiac reflexes (Smith and Thames, 1994), which affect vagal efferent nerve activity. As an example, activation of Bezold–Jarisch reflex by intravenous phenylbiguanide increases myocardial interstitial ACh level (Kawada et al., 2001b). Such reflexes from the heart may participate in the brief ischaemia-induced myocardial interstitial ACh release.

Brief ischaemia increased the myocardial interstitial NA levels in neither the INT-BI nor VX-BI group (Fig. 3, $B_1$ and $B_2$). The lack of NA release during brief ischaemia is consistent with a study in isolated perfused rat hearts (Seyfarth et al., 1996). When the isolated rat heart is perfused with buffer containing glucose, an ischaemic period of more than 10 min is required for myocardial NA release associated with energy depletion (Schömig et al., 1987). Aside from the energy depletion, reflexes from the heart may also affect myocardial interstitial NA level in vivo. While cardiac sympathetic reflex exerts sympatho-excitatory effects, cardiac vagal reflex exerts sympatho-inhibitory effects (Hainsworth, 1991). The lack of NA release may indicate that the cardiac vagal reflex predominates over the cardiac sympathetic reflex during the brief ischaemia in the present experimental settings.

### *4.2. Effects of 60-min ischaemia on myocardial ACh release*

The INT-BI but not VX-BI group showed more enhanced ACh release than the INT group during the last 15 min of

Table 2
Changes in heart rate (HR) and mean arterial pressure (MAP) in VX-BI group

| | C | $B_1$ | $B_2$ | $S_1$ | $S_2$ | $S_3$ | $S_4$ | R |
|---|---|---|---|---|---|---|---|---|
| HR (beats/min) | 179.5 ± 10.2 | 191.5 ± 7.3 | 183.0 ± 8.4 | 178.8 ± 9.2 | 183.0 ± 7.8 | 180.8 ± 7.4 | 180.5 ± 8.0 | 181.5 ± 7.7 |
| MAP (mm Hg) | 150.3 ± 7.3 | 148.5 ± 4.0 | 143.3 ± 8.0 | 138.5 ± 7.4 | 134.3 ± 8.4[a] | 130.7 ± 8.2[a] | 135.2 ± 5.6[b] | 127.7 ± 7.5[a] |

Values are means ± SEM.
Data were obtained during control (C), after 5 min of each brief ischaemia ($B_1$ and $B_2$), after 5, 30, 45 and 60 min of sustained ischaemia ($S_1$, $S_2$, $S_3$ and $S_4$), and after 5 min of reperfusion (R).
[a] $P<0.01$ from control.
[b] $P<0.05$ from control.

the 60-min ischaemia (Fig. 4A). The maximum ACh level in the INT-BI group exceeded the myocardial interstitial ACh level observed in response to 20-Hz electrical vagal stimulation in our previous study (Kawada et al., 2001b). Electrical vagal stimulation protects the heart from lethal ventricular arrhythmias associated with acute myocardial ischaemia in anaesthetized cats (Rosenshtraukh et al., 1994). Thus, brief ischaemia may enhance the myocardial interstitial ACh release during subsequent ischaemia, thereby augmenting ameliorative effects of the vagal system on the ischaemic myocardium.

Several mechanisms can be put forward to explain the myocardial interstitial ACh release during sustained ischaemia. Firstly, myocardial ischaemia evokes cardiac vagal reflexes such as the Bezold–Jarisch reflex, thereby increased vagal efferent nerve activity. Secondly, myocardial ischaemia caused axonal reflex or intracardiac ganglionic reflex and modified postganglionic vagal nerve activity independent of efferent signals from the medulla (Foreman, 1994; Armour, 1999). Thirdly, myocardial ischaemia evokes ACh release from vagal nerve terminal independent of postganglionic vagal nerve activity. The fact that vagotomy at the neck failed to abolish the sustained ischaemia-induced ACh release (Fig. 2, VX-BI) indicates that the latter two mechanisms play important roles for the sustained ischaemia-induced ACh release.

With respect to the mechanisms responsible for the enhanced ACh release during subsequent ischaemia in the INT-BI group, HR did not decrease progressively, contrasting with the progressive increase in the ACh levels during subsequent ischaemia (Table 1). If we assume that changes in HR reflected vagal efferent nerve activity to the heart, the ACh response deviated from the vagal efferent nerve activity. Thus, we speculate that brief ischaemia enhanced the regional ACh release during subsequent ischaemia via the second and third mechanisms independent of efferent signals from the medulla.

### *4.3. Effects of 60-min ischaemia on myocardial NA release*

Previous studies indicated that brief ischaemia reduces cardiac NA release during subsequent sustained ischaemia in isolated rat hearts (Seyfarth et al., 1996; Feng et al., 1997). Although we expected that brief ischaemia would reduce myocardial interstitial NA release during sustained ischaemia, the myocardial interstitial NA levels did not differ between the INT-BI and INT groups (Fig. 4B). However, if we compare the NA levels in the vagotomized groups (VX-BI vs. VX groups), the brief ischaemia attenuated the NA release during sustained ischaemia. Taking into account the fact that the isolated rat hearts is free of vagal innervation, the results from vagotomized groups in the present study appears to be consistent with the results obtained from the isolated rat heart. Because vagal afferent fibers exert sympatho-inhibitory effects during acute myocardial ischaemia, sustained ischaemia-induced NA release is suppressed even without preceding brief ischaemia when vagi are kept intact (Kawada et al., 2001a). As a result, the effects of brief ischaemia on subsequent ischaemia-induced NA release would be uncovered only in animals with vagotomy.

Other factors that can be involved in the effects of brief ischaemia on subsequent ischaemia-induced NA and ACh release are prejunctional interactions. In the prejunctional interactions, NA acts on vagal nerve terminals and inhibits ACh release (Wetzel et al., 1985), whereas ACh acts on sympathetic nerve terminals and inhibits NA release (Manabe et al., 1991). However, according to the results of our previous study (Kawada et al., 2001a), α-adrenergic blockade by phentolamine administration did not affect ischaemia-induced ACh release. Similarly, muscarinic blockade by atropine did not affect ischaemia-induced NA release. Therefore, the role of prejunctional interactions in the ischaemia-induced neurotransmitter release in the ischaemic myocardium would be minimal.

### *4.4. Limitations*

Although cardiac microdialysis was useful for analyzing neural regulation at cardiac nerve terminals, there were several limitations to the present study. Firstly, we investigated myocardial interstitial ACh and NA levels in cats anaesthetized with pentobarbital sodium. As the anaesthesia affects the autonomic nervous system, the results might have differed had the experiment been performed in conscious animals. Secondly, we administered eserine through the dialysis probe. As ACh released from the vagal nerve terminal is immediately degraded (Nicholls, 1994), cholinesterase inhibition was necessary to detect changes in myocardial interstitial ACh levels. Thus, the possibility cannot be ruled out that eserine modified ACh release from the vagal nerve terminals. Although eserine may also affect ganglionic transmission, Akiyama et al. (1994) demonstrated that local administration of hexamethonium through the dialysis probe did not inhibit the ACh response to electrical vagal stimulation. Thus, ventricular area penetrated by the dialysis probe in the present study would not have contained many ganglia. Thirdly, functional roles of the observed changes in myocardial interstitial ACh and NA levels were not examined in the present study. Although myocardial ischaemic preconditioning has been reported in many species including dogs, rats, rabbits, and pigs (Reimer and Jennings, 1992), only a few studies reported the myo-cardial ischaemic preconditioning in cats (Na et al., 1996; Pan et al., 2000). The lack of information makes it difficult to further speculate the relationship between myocardial ischaemic preconditioning and brief ischaemia-induced changes in neurotransmitter release. Further studies are clearly needed to elucidate the functional significance of the neural regulation during brief ischaemia and subsequent sustained ischaemia.

### 4.5. Conclusion

Brief ischaemia increased myocardial interstitial ACh level in the ischaemic region. Brief ischaemia also enhanced myocardial interstitial ACh release during subsequent sustained ischaemia. Since vagal stimulation protects the heart from lethal arrhythmia associated with myocardial ischaemia (Rosenshtraukh et al., 1994), the enhanced ACh release during sustained ischaemia may exert ameriolative effects on the heart. In contrast to the vagal system, the effects of brief ischaemia on myocardial interstitial NA release during sustained ischaemia were evident only in vagotomized animals.

## Acknowledgements

This study was supported by Research Grants from the Ministry of Health and Welfare of Japan, Cardiovascular Diseases (9C-1, 11C-3, 11C-7), Health Sciences Research Grant for Advanced Medical Technology; a Grant from NASDA (National Space Development Agency of Japan) and Japan Space Forum, Ground-Based Research Grant for the Space Utilization; a Grant from the Science and Technology Agency of Japan, Bilateral International Joint Research Grant; Grants from the Ministry of Education, Science, Sports and Culture of Japan, Grant-in-Aid for Scientific Research (B-11694337, C-11680862, C-11670730) and Grant-in-Aid for Encouragement of Young Scientists (11770390, 11770391); and a Grant from Japan Science and Technology, Research and Development for Applying Advanced Computational Science and Technology.

## References

Akiyama, T., Yamazaki, T., Ninomiya, I., 1991. In vivo monitoring of myocardial interstitial norepinephrine by dialysis technique. Am. J. Physiol. 261, H1643–H1647.

Akiyama, T., Yamazaki, T., Ninomiya, I., 1994. In vivo detection of endogenous acetylcholine release in cat ventricles. Am. J. Physiol. 266, H854–H860.

Armour, J.A., 1999. Myocardial ischaemia and the cardiac nervous system. Cardiovasc. Res. 41, 41–54.

Dawson, V.L., Dawson, T.M., 2000. Neuronal ischaemic preconditioning. Trends Pharmacol. Sci. 21, 423–424.

Feng, J., Yamaguchi, N., Foucart, S., Chahine, R., Lamontagne, D., Nadeau, R., 1997. Transient ischemia inhibits nonexocytotic release of norepinephrine following sustained ischemia in rat heart: is bradykinin involved? Can. J. Physiol. Pharmacol. 75, 665–670.

Foreman, R.D., 1994. Spinal cord neuronal regulation of the cardiovascular system. In: Armour, J.A., Ardell, J. (Eds.), Neurocardiology. Oxford Univ. Press, pp. 245–276.

Glantz, S.A., 1997. Primer of Biostatistics, 4th edn. McGraw-Hill, New York.

Kawada, T., Yamazaki, T., Akiyama, T., Sato, T., Shishido, T., Yoshimura, R., Inagaki, M., Tatewaki, T., Sugimachi, M., Sunagawa, K., 1999. Local epinephrine release in the rabbit myocardial interstitium in vivo. J. Auton. Nerv. Syst. 78, 94–98.

Kawada, T., Yamazaki, T., Akiyama, T., Sato, T., Shishido, T., Inagaki, M., Takaki, H., Sugimachi, M., Sunagawa, K., 2000. Differential acetylcholine release mechanisms in the ischemic and nonischemic myocardium. J. Mol. Cell. Cardiol. 32, 405–414.

Kawada, T., Yamazaki, T., Akiyama, T., Inagaki, M., Shishido, T., Zheng, C., Yanagiya, Y., Sugimachi, M., Sunagawa, K., 2001a. Vagosympathetic interactions in ischemia-induced myocardial norepinephrine and acetylcholine release. Am. J. Physiol.: Heart Circ. Physiol. 280, H216–H221.

Kawada, T., Yamazaki, T., Akiyama, T., Shishido, T., Inagaki, M., Uemura, K., Miyamoto, T., Sugimachi, M., Takaki, H., Sunagawa, K., 2001b. In vivo assessment of acetylcholine releasing function at cardiac vagal nerve terminals. Am. J. Physiol.: Heart Circ. Physiol. 281, H139–H145.

Hainsworth, R., 1991. Reflexes from the heart. Physiol. Rev. 71, 617–658.

Manabe, N., Foldes, F.F., Töröcsik, A., Nagashima, H., Goldiner, P.L., Vizi, E.S., 1991. Presynaptic interaction between vagal and sympathetic innervation in the heart: modulation of acetylcholine and noradrenaline release. J. Auton. Nerv. Syst. 32, 233–242.

Murry, C.E., Jennings, R.B., Reimer, K.A., 1986. Preconditioning with ischemia: a delay of lethal cell injury in ischemic myocardium. Circulation 74, 1124–1136.

Na, H.S., Kim, Y.I., Yoon, Y.W., Han, H.C., Nahm, S.H., Hong, S.K., 1996. Ventricular premature beat-driven intermittent restoration of coronary blood flow reduces the incidence of reperfusion-induced ventricular fibrillation in a cat model of regional ischemia. Am. Heart J. 132, 78–83.

Nicholls, D.G., 1994. Proteins, Transmitters and Synapses. Blackwell, Oxford, UK, pp. 186–199.

Pan, H.L., Chen, S.R., Scicli, G.M., Carretero, O.A., 2000. Cardiac interstitial bradykinin release during ischemia is enhanced by ischemic preconditioning. Am. J. Physiol.: Heart Circ. Physiol. 279, H116–H121.

Reimer, K.A., Jennings, R.B., 1992. Preconditioning. Definitions, proposed mechanisms, and implications for myocardial protection in ischemia and reperfusion. In: Yellon, D.M., Jennings, R.B. (Eds.), Myocardial Protection. The Pathophysiology of Reperfusion and Reperfusion Injury. Raven Press, New York, pp. 165–183.

Rosenshtraukh, L., Danilo Jr., P., Anyukhovsky, E.P., Steinberg, S.F., Rybin, V., Brittain-Valenti, K., Molina-Viamonte, V., Rosen, M.R., 1994. Mechanisms for vagal modulation of ventricular repolarization and of coronary occlusion-induced lethal arrhythmias in cars. Circ. Res. 75, 722–732.

Schömig, A., Fischer, S., Kurz, T., Richardt, G., Schömig, E., 1987. Non-exocytotic release of endogenous noradrenaline in the ischemic and anoxic rat heart: mechanism and metabolic requirements. Circ. Res. 60, 194–205.

Seyfarth, M., Richardt, G., Mizsnyak, A., Kurz, T., Schömig, A., 1996. Transient ischemia reduces norepinephrin release during sustained ischemia. Neural preconditioning in isolated rat heart. Circ. Res. 78, 573–580.

Smith, M.L., Thames, M.D., 1994. Cardiac receptors: discharge characteristics and reflex effects. In: Armour, J.A., Ardell, J. (Eds.), Neurocardiology. Oxford Univ. Press, pp. 19–52.

Wetzel, G.T., Goldstein, D., Brown, J.H., 1985. Acetylcholine release from rat atria can be regulated through an α1-adrenergic receptor. Circ. Res. 56, 763–766.

Yamazaki, T., Akiyama, T., Kitagawa, H., Takauchi, Y., Kawada, T., Sunagawa, K., 1997. A new, concise dialysis approach to assessment of cardiac sympathetic nerve terminal abnormalities. Am. J. Physiol. 272, H1182–H1187.

Yamazaki, T., Akiyama, T., Kawada, T., Kitagawa, H., Takauchi, Y., Yahagi, N., Sunagawa, K., 1998. Norepinephrine efflux evoked by potassium chloride in cat sympathetic nerves: dual mechanism of action. Brain Res. 794, 146–150.

Yamazaki, T., Akiyama, T., Kawada, T., 1999. Effects of ouabain on in situ cardiac sympathetic nerve endings. Neurochem. Int. 35, 439–445.

*Am J Physiol Heart Circ Physiol* 283: H2687–H2691, 2002.
First published August 29, 2002; 10.1152/ajpheart.00291.2002.

# Disruption of vagal efferent axon and nerve terminal function in the postischemic myocardium

TORU KAWADA,[1] TOJI YAMAZAKI,[2] TSUYOSHI AKIYAMA,[2]
HIDEZO MORI,[2] KAZUNORI UEMURA,[1] TADAYOSHI MIYAMOTO,[1]
MASARU SUGIMACHI,[1] AND KENJI SUNAGAWA[1]
[1]*Departments of Cardiovascular Dynamics and* [2]*Cardiac Physiology, National Cardiovascular Center Research Institute, Osaka 565–8565, Japan*

Received 25 February 2002; accepted in final form 22 August 2002

**Kawada, Toru, Toji Yamazaki, Tsuyoshi Akiyama, Hidezo Mori, Kazunori Uemura, Tadayoshi Miyamoto, Masaru Sugimachi, and Kenji Sunagawa.** Disruption of vagal efferent axon and nerve terminal function in the postischemic myocardium. *Am J Physiol Heart Circ Physiol* 283: H2687–H2691, 2002. First published August 29, 2002; 10.1152/ajpheart.00291.2002.—Despite the importance of vagal control over the ventricle, little is known regarding vagal efferent conduction and nerve terminal function in the postischemic myocardium. To elucidate postischemic changes in the cardiac vagal efferent neuronal function, we measured myocardial interstitial acetylcholine (ACh) levels by using in vivo cardiac microdialysis and examined the ACh responses to electrical stimulation of the vagi or local administration of ouabain in anesthetized cats. Sixty-minute occlusions of the left anterior descending coronary artery (LAD) followed by 60-min reperfusion abolished electrical stimulation-induced ACh release (20.4 ± 3.9 vs. 0.9 ± 0.4 nmol/l; means ± SE, $P < 0.01$). In different groups of animals, 60-min LAD occlusion followed by 60-min reperfusion decreased but did not completely abolish ouabain-induced release of ACh (9.2 ± 1.8 vs. 3.9 ± 0.7 nmol/l; $P < 0.05$). These results indicate that function of the vagal efferent axon was completely interrupted, whereas the local ACh release was partially suppressed in the postischemic myocardium. The postischemic disruption of vagal efferent neuronal function might exert deleterious effects on cardiac regulation.

cardiac microdialysis; vagal stimulation; ouabain; cats; acetylcholine

AUTONOMIC DERANGEMENT ASSOCIATED with acute myocardial ischemia or infarction has deleterious effects on the heart (3, 6). The autonomic derangement occurs during postischemic as well as ischemic periods. Elucidating the underlying mechanisms of autonomic disturbance during the postischemic period is important to understand the pathophysiology of postischemic events such as those occurring after thrombolytic therapies. In the sympathetic nervous system, nerve terminal function as assessed by tyramine-induced norepinephrine release recovers 60–120 min after reperfusion of the coronary artery (1, 14). On the other hand, the myocardial response to electrical stimulation of sympathetic efferent neurons remains impaired up to 2 h after reperfusion, despite a preserved myocardial response to exogenous norepinephrine (5). Therefore, injury to sympathetic efferent axons (4, 8) is considered to be responsible for sympathetic denervation in the postischemic myocardium. However, conduction of the postganglionic axons in response to electrical stimulation of the epicardial sites was unaffected by regional ventricular ischemia (9), suggesting that the intrinsic cardiac fibers in the epicardial region were resistant to myocardial ischemia. We speculate that changes in the environment surrounding the postganglionic axons traveling through the midcardium affected the axonal conduction (15) even if the axon itself was not injured.

In contrast to the sympathetic efferent nervous system, little is known regarding vagal efferent neuronal function in the postischemic myocardium in vivo. We have measured myocardial interstitial acetylcholine (ACh) levels by using a cardiac microdialysis technique in anesthetized cats (2, 10–13). The ACh levels measured by the cardiac microdialysis were able to detect changes in the ACh kinetics in the vagal nerve terminals induced by pharmacological interventions, arterial baroreflex, or Bezold-Jarisch reflex (13). ACh levels increased during 60-min occlusion of the left anterior descending coronary artery (LAD) and decreased toward preocclusion level after LAD reperfusion (12). Whether the reduction in the ACh level on reperfusion indicated functional recovery of ACh release in the postischemic myocardium remains to be elucidated.

The purpose of the present study was to examine ACh release in the postischemic myocardium. We employed two methods of vagal stimulation to induce myocardial ACh release: electrical stimulation of the vagi and local administration of ouabain. We assumed that the ACh response to electrical stimulation reflected efferent neuronal function including both axonal conduction and local ACh release from the vagal nerve terminals. In contrast, the ACh response to local ouabain administration was considered to reflect the

Address for reprint requests and other correspondence: T. Kawada, Dept. of Cardiovascular Dynamics, National Cardiovascular Center Research Institute, 5-7-1 Fujishirodai, Suita, Osaka 565-8565, Japan (E-mail: torukawa@res.ncvc.go.jp).

The costs of publication of this article were defrayed in part by the payment of page charges. The article must therefore be hereby marked "*advertisement*" in accordance with 18 U.S.C. Section 1734 solely to indicate this fact.

  

local ACh release from the vagal nerve terminals alone. Results indicate that vagal efferent axonal conduction was interrupted, and local ACh release was suppressed in the postischemic myocardium 60 min after reperfusion after 60-min LAD occlusion.

## MATERIALS AND METHODS

*Surgical preparations.* Animal care was provided in accordance with the *Guiding Principles for the Care and Use of Animals in the Field of Physiological Sciences* approved by the Physiological Society of Japan. A total of 37 adult cats was anesthetized via an intraperitoneal injection of pentobarbital sodium (30–35 mg/kg) and ventilated mechanically with room air mixed with oxygen. The depth of anesthesia was maintained with a continuous intravenous infusion of pentobarbital sodium (1–2 $mg \cdot kg^{-1} \cdot h^{-1}$) through a catheter inserted from the right femoral vein. Systemic arterial pressure was measured from a catheter inserted into the right femoral artery. Heart rate (HR) was determined by using a cardiotachometer from an electrocardiogram. Esophageal temperature of the animal was measured by using a thermometer (model CTM-303; Terumo) and was maintained at around 37°C by using a heated pad and a lamp.

With the animal in the lateral position, the left fifth and sixth ribs were resected to expose the heart. A dialysis probe was implanted by inserting a fine guiding needle into the anterolateral free wall of the left ventricle perfused by the LAD (1, 2, 10–13, 20, 21). Heparin sodium (100 U/kg) was administered intravenously to prevent blood coagulation. When LAD occlusion was required, a 4-0 silk suture was passed around the LAD just distal to the first diagonal branch, and both of its ends were passed through a polyethylene tube to make a snare for occlusion. The discoloration area on the LAD occlusion was large enough to cover the full length of the implanted dialysis fiber macroscopically. When vagal stimulation was required, the vagi were exposed bilaterally in the neck. Bipolar platinum electrodes were then attached to the cardiac end of each sectioned vagal nerve. The nerves and electrodes were covered with warmed mineral oil for insulation. A pair of stainless steel wire electrodes was attached to the left ventricular apex removed from the implanted dialysis probe to pace the heart during electrical stimulation of the vagi.

At the end of the experiment, the experimental animals were killed with an overdose of pentobarbital sodium. Postmortem examination confirmed that the dialysis probe had been implanted within the left ventricular myocardium.

*Dialysis technique.* We measured the concentration of ACh in the dialysate sample as an index of myocardial interstitial ACh level (10–13). Materials and properties of the dialysis probe have been reported previously (2). Briefly, we designed a transverse dialysis probe. A dialysis fiber (13-mm length, 310 μm OD, 200 μm ID; 50,000 molecular weight cutoff) (model PAN-1200; Asahi Chemical, Japan) was glued at both ends to polyethylene tubes (25-cm length, 500 μm OD, 200 μm ID). The dialysis probe was perfused at a rate of 2 μl/min with Ringer solution containing a cholinesterase inhibitor, eserine (100 μM). Experimental protocols were initiated 2 h after implanting the dialysis probe. The dialysate sampling period was set at 15 min and was performed taking into account the dead space volume between the dialysis membrane and the sample tube. Concentration of ACh in the dialysate was measured by high performance liquid chromatography with electrochemical detection (Eicom).

*Protocols.* Acute myocardial ischemia was induced by LAD occlusion. The study consisted of the following two different protocols (Fig. 1). In *protocol 1*, the myocardial interstitial ACh response to electrical stimulation of the vagi was examined (2, 13). Fifteen-minute vagal stimulation (20 Hz, 1 ms pulse duration, 10 V pulse amplitude) was performed under ventricular pacing at 200 beats/min in the following groups of vagotomized animals: control ($n$ = 7), 15-min ischemia followed by 60-min reperfusion ($CO_{15}$ group, $n$ = 5), and 60-min ischemia followed by 60-min reperfusion ($CO_{60}$ group, $n$ = 5). Pacing was applied only during the vagal stimulation and not during the ischemic period.

In *protocol 2*, the myocardial interstitial ACh response to local ouabain administration was examined (13, 20). We collected a baseline dialysate sample while perfusing the dialysis probe with Ringer solution. We then replaced the perfusate with Ringer solution containing ouabain (100 μM),

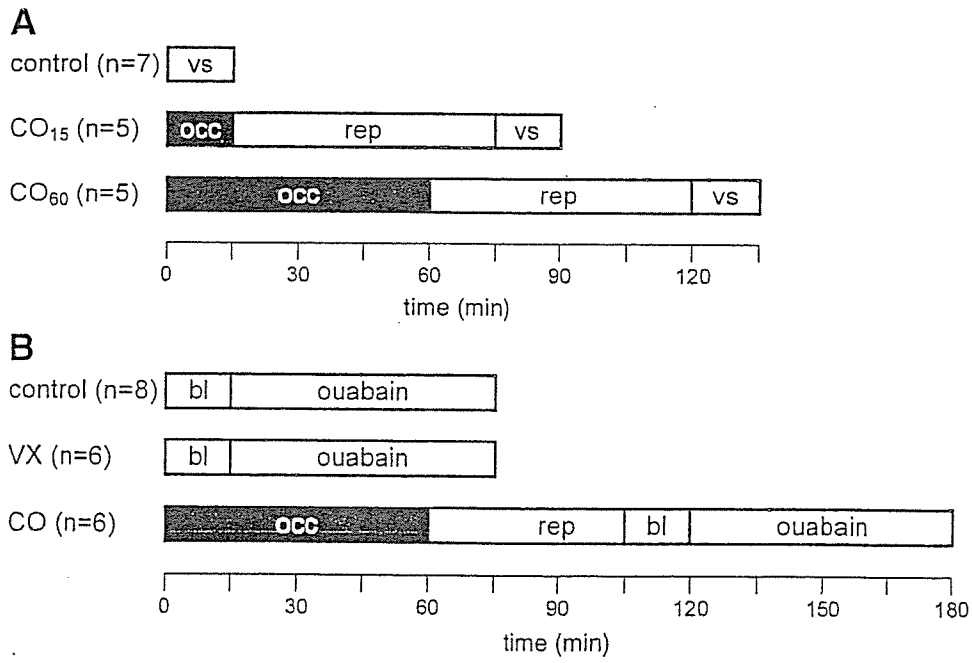


Fig. 1. Experimental protocols. *Protocol 1* (*A*) was performed on vagotomized animals. Effects of electrical vagal stimulation on myocardial interstitial ACh level were examined in three groups of animals: control; 15-min ischemia followed by 60-min reperfusion ($CO_{15}$); and 60-min ischemia followed by 60-min reperfusion ($CO_{60}$). *Protocol 2* (*B*) was performed on animals different from those in *Protocol 1*. Effects of local ouabain administration on myocardial interstitial ACh level were examined in three groups of animals: control (intact vagi); vagotomized (VX); and 60-min ischemia followed by 60-min reperfusion with intact vagi (CO). occ, Occlusion of the left anterior descending coronary artery; rep, reperfusion after occlusion; vs, vagal stimulation; bl, baseline before ouabain administration.